Journal of Materials Science, 2007, vol. 42, 6353-6370

Crack Growth in Structural Adhesive Joints in Aqueous Environments

A. J. KINLOCH, C.F. KORENBERG[1] and K.T. TAN[2]

Department of Mechanical Engineering, Imperial College London, Exhibition Road, London SW7 2AZ, UK.

and J. F. WATTS

The Surface Analysis Laboratory, School of Engineering, University of Surrey, Guildford, Surrey, GU2 7XH, UK.

The adhesive fracture energy, G_c, of metallic joints, bonded with a rubber-toughened epoxy adhesive, has been measured using monotonically-loaded tests. Such tests have been conducted in various relative humidities and in water, at 21°C. Two surface pretreatments have been employed for the substrates prior to bonding: a simple grit-blast and degrease ('GBD') pretreatment or a grit-blast, degrease and silane primer ('GBS') pretreatment. The joints were formed using metallic substrates which were either (a) aluminium-alloy substrates, (b) steel substrates, or (c) 'dissimilar' substrates (i.e. one substrate being aluminium-alloy with the other one being steel). For both test environments, when G_c was plotted against the crack velocity, three regions of fracture behaviour could be distinguished. At low rates of displacement the crack grew in a stable manner, visually along the interface, and relatively low crack velocities could be readily measured. This was termed 'Region I' and here the value of G_c measured in the aqueous environment was relatively low compared to that measured in a relatively dry environment of 55% relative humidity. On the other hand, at relatively high rates of displacement the crack always grew in a stick-slip manner mainly cohesively in the adhesive layer at approximately 20 km/minute. This was termed 'Region III', and here the value of G_c was relatively high and independent of the environmental test conditions employed. In this region the crack was considered to grow faster than the water molecules were able to reach the crack tip, which explains the independence of G_c upon the test environment. In between 'Region I' and 'Region III', a transition region was observed which was designated as 'Region II'. The major effect of the 'GBS' pretreatment, compared to the 'GBD' pretreatment, was to increase the value of G_c both in 'Regions I and III', although the presence of the silane primer had the far greater effect in 'Region I'.

---

[1] Current address: British Museum, Great Russell Street, London WC1B 3DG, UK
[2] Current address: NIST, 100 Bureau Drive, Gaithersburg, MD 20899-8615, USA

Keywords: Accelerated testing, Durability, Environmental attack, Fracture mechanics, Silane primer, Structural adhesives.

1. INTRODUCTION

There are many advantages that polymeric adhesives can offer compared to the more traditional methods of joining such as bolting, brazing, welding, mechanical fasteners, etc. These include [1-3] the ability to join dissimilar materials to give light-weight, but strong and stiff, structures, such as honeycomb sandwich panels. Also, polymeric adhesives may be used to join thin-sheet material efficiently. Further, adhesive bonding frequently represents the most convenient and cost-effective joining technique and, indeed, the bonding operation can often be readily automated. For these reasons, adhesive bonding is widely used in the aerospace, automotive and electronics industries.

However, a major concern is that the mechanical performance of structural adhesive joints involving metallic or ceramic substrates may deteriorate upon being exposed to aqueous environments [1-3]. Further, these previous reviews have revealed that it is the interphase of the joint, i.e. the region adjacent to the interface between the substrate and the polymeric adhesive, which is susceptible to such attack and on which attention must be focussed. Nevertheless, there are several problems which remain to be overcome. For example, the development of (a) a sound accelerated (i.e. short-term) test methods to assess the long-term durability of adhesive joints and (b) improved 'environmentally-friendly' surface pretreatments to improve joint durability are of great interest.

The present research was therefore undertaken with several main objectives. A first objective was to investigate the use of monotonically-loaded tests as an accelerated ageing method for assessing the joint durability in both humid and aqueous (i.e. liquid water) environments. A second objective was to employ this test method to investigate any improvement in the joint durability that might be obtained by the use of a silane primer as a surface pretreatment prior to bonding, this treatment being of special interest since it is an

'environmentally-friendly' treatment method. A third major objective was to identify the mechanisms of any environmental attack which was observed. Since only by such mechanisms being elucidated will improved accelerated test methods and new, more effective. surface pretreatments be developed.

The basic approach taken in the present research has been to employ a fracture-mechanics tests, using a tapered double-cantilever beam (TDCB) specimen, and the essence of the test procedure has been the examination of the failure behaviour over a wide range of rates of displacement. The joints were formed using a commercially-available rubber-toughened epoxy adhesive to bond metallic substrates which were either (a) aluminium-alloy substrates, (b) steel substrates, or (c) 'dissimilar' substrates (i.e. one substrate being aluminium-alloy with the other one being steel). In addition to ascertaining the value of the adhesive fracture energy, G_c, for the different joints in the various test environments as a function of the corresponding crack velocity, $\dot{a}$, the loci of failure have been assessed using scanning electron microscopy (SEM), X-ray photoelectron spectroscopy (XPS) and time-of-flight secondary ion mass spectroscopy (ToF-SIMS) to help identify the mechanisms of failure.

2. EXPERIMENTAL

2.1 Materials and Surface Pretreatments

The adhesive employed was a hot-cured rubber-toughened epoxy-paste adhesive that was based upon a diglycidyl ether of bisphenol-A epoxy cured with dicyandiamide. The substrates were manufactured from either steel (Grade BS 970 070M55) or aluminium alloy (Grade BS 7075 (unclad)). Their compositions are given in Tables 1 and 2 respectively.

For both types of substrate, two different surface pretreatments prior to bonding were employed. The first surface pretreatment consisted of degreasing the substrates in a liquid bath of

boiling 1,1,1-trichloroethylene which was followed by grit-blasting using 60μm-78μm mesh alumina particles. The substrates were then vapour degreased above a bath of boiling trichloroethylene and allowed to cool to room temperature. This pretreatment is denoted as the 'GBD' pretreatment. In the second pretreatment employed, the previous grit-blasting and degreasing procedures were first undertaken which was then followed by the application of a silane-based primer, to give the 'GBS' pretreatment; i.e. a grit-blast silane surface pretreatment. A 1%w/w solution of γ-glycidoxypropyltrimethoxy silane (GPS) solution, using a 90:10 by weight of ethanol:deionised water mixture, was prepared and its pH was adjusted to approximately five by the addition of acetic acid. This solution was stirred for 60 minutes to allow complete hydrolysis of the GPS to occur. The solution was then painted onto the surfaces of the substrates that were to be bonded, using a small brush. The substrates were drained onto a tissue and the GPS layer was cured at 93^{o}C for 60 minutes. This procedure is very similar to that recommended by Digby and Shaw [4].

2.2 Joint Preparation

To determine the adhesive fracture energy, G_c, an adhesively-bonded tapered double-cantilever beam (TDCB) specimen was employed, as described below. At the end of the substrates where the load was to be applied, a thin layer of silicon-based release agent ("Frekote 770-NC", Henkel, UK) was painted over a length of about 90 mm of the substrate surface to act as a precrack. Applying the release agent with a 'chevron-shaped' end was found to give a precrack that tended to promote stable failure, as opposed to unstable failure, as described below.

The adhesive was degassed under vacuum for a short time at 80^{o}C and was then applied to the faces of the substrates to be bonded using a spatula. The thickness of the adhesive layer was 0.4 mm and was controlled via thin steel wires inserted into either end of the TDCB specimen.

The adhesive layer was cured by heating the adhesive for two hours at 130^{o}C, as monitored via an *in-situ* thermocouple, and the joints were then cooled in the oven overnight.

2.3 Fracture-Mechanics Tests

To determine the adhesive fracture energy, G_C, an adhesively-bonded tapered double-cantilever beam (TDCB) specimen was employed. The value of the adhesive fracture energy, G_C, was determined using the expression [5]:

$$G_C = \frac{P_c^2}{2b} \cdot \frac{dC}{da} \tag{1}$$

where P_c is the critical load for crack growth as discussed below, a is the crack length, b is the width of the specimen and C is the compliance of the specimen ($C = y/P$; where y is the displacement and P is the load). Now, for the similar-substrate joints, where both substrates were either aluminium alloy or steel, the beams were contoured to give a value of the geometry constant, m, of 2mm^{-1}. However, when dissimilar-substrate joints were employed, then the steel substrate was contoured as before but the aluminium-alloy substrates were contoured with a value of m of 0.70 mm^{-1}. This was done to account for the differences in the stiffnesses of the dissimilar substrates; where the value of m is given by:

$$m = \frac{3a^2}{h^3} + \frac{1}{h} \tag{2}$$

where h is the height of the beam at a corresponding crack length, a. The beams were 310mm in length, with the height, h, having a value of 32 mm at a crack length, a, of 150 mm. The width, b, of the beams was 10mm.

Tests were conducted at a constant rate of displacement, $\dot{y}$, of the crosshead of the tensile testing machine and the crack length, *a*, was monitored as a function of time using a video camera. The rate of displacement used for these monotonically-loaded tests was varied between 0.005 to 10 mm/minute. The tests were conducted at 21±1°C in an environmental chamber which permitted a wide range of relative humidities to be employed, as well as tests to be undertaken in water. The relative humidity, RH, in the environmental chamber was controlled using various salt solutions [6] and was measured using a hair hygrometer. The experimentally measured RH values were in close agreement with the expected RH values, see Table 3. In the case of the tests undertaken in water, then the chamber was filled with water at 21±1°C to just above the top of the TDCB bonded joint, and the specimen allowed to equilibrate for about twelve hours prior to the test commencing. From these fracture-mechanics tests the value of the adhesive fracture energy, G_c, for the different joints in the various test environments could be determined as a function of the corresponding crack velocity, $\dot{a}$.

2.4 Examination of the Fracture Surfaces

In the present work three experimental techniques were employed to study the surfaces of the specimens. Firstly, a 'JEOL JSM 5300' scanning electron microscope was used to examine the surfaces of the fractured joints. Secondly, since it is not always possible to determine with certainty the locus of failure using a scanning electron microscope (for example, a very thin layer of adhesive or oxide would not be detectable), X-ray photoelectron spectroscopy (XPS) was also employed. The apparatus used in the present study was a 'Thermo VG Scientific Sigma Probe' spectrometer, equipped with both a monochromatic AlKα source and an achromatic AlKα/MgKα twin anode assembly. The monochromatic source was employed in this work operating in the large area mode which provides an X-ray spot size of 500μm, charge neutralisation was carried out using an electron flood gun. Survey spectra were acquired with a pass energy of 100 eV and

the high resolution spectra with a pass energy of 50 eV. Quantitative surface chemical analyses and peak fitting were undertaken on the high resolution spectra using the software provided by the manufacturer. Thirdly, time-of-flight secondary ion mass spectroscopy (ToF-SIMS) was also employed and spectra were recorded using a VG Scientific Type 23 system equipped with a pulsed Ga^+ source and a two stage reflectron analyser. Spectra were acquired over a 500 μm x 500 μm area. The gallium source was operated at a pulse rate of 50 kHz and pulse width of 25 ns; total ion dose was kept below the static limit of 10^{12} ions cm^{-2} $analysis^{-1}$.

3. CRACK PROPAGATION STUDIES

3.1 The Relationship Between G_c and $\dot{a}$

Before considering the effects of the test environment on the bonded joints in detail, it is useful to consider the general form of the relationships which were obtained between the adhesive fracture energy, G_c, and the corresponding crack velocity, $\dot{a}$. These relationships are shown in Figures 1 to 3 for the (a) aluminium-alloy, (b) steel and (c) aluminium alloy-steel dissimilar joints, respectively, that were tested at 21±1°C in 55% RH (which was the ambient RH in the air-conditioned laboratory) and for immersion in water. In these figures the data are plotted in the form of $\log_{10} G_c$ versus $\log_{10} \dot{a}$. Also, results for the two pretreatments (i.e. the 'GBD' and 'GBS') are given for all types of joints.

For all the joints studied, and in both test environments, three different regions of crack growth behaviour may be identified and these have been labelled 'Region I', 'Region II' and 'Region III', in the spirit of the classic studies of Wiederhorn [7] on crack growth in glass. 'Region I' occurred at relatively low rates of displacement and the fracture was stable in nature and was visually interfacial, whereas 'Region III' was observed at relatively high rates of displacement and the fracture was unstable and essentially cohesive in the adhesive layer. 'Region II' was the transition region between 'Region I' and 'Region III'. It should be noted that

previous researchers [8-14] have also reported results from studies on the sub-critical crack growth in epoxy-bonded joints which follow the general pattern reported by Wiederhorn [7].

3.2 'Region I' Behaviour

This region was observed at relatively low rates of displacement, $\dot{y}$, and the crack propagated in a stable manner visually along the substrate/adhesive interface. (It should be noted that the dissimilar joints always failed visually along the steel-adhesive interface, as opposed to the aluminium alloy-adhesive interface.) During crack growth in 'Region I', the load was essentially constant at a value of P_c, and a typical load, P, versus displacement, y, curve associated with stable crack growth is shown in Figure 4. The average value of the load, P_c, for crack growth was employed to determine the value of the adhesive fracture energy, G_c, as indicated above (see Equation (1)).

For a test at a given rate of displacement, $\dot{y}$, the relationship between crack length, a, and time, t, was linear as shown in Figure 5 which leads, of course, to a constant value of the crack velocity, $\dot{a}$, throughout the test, as the crack propagates down the length of the TDCB specimen. The higher the rate of displacement employed within 'Region I', then the higher the resulting crack velocity, as illustrated in Figure 6. Thus, for a given joint system, the crack velocity, $\dot{a}$, is controlled by the rate of displacement, $\dot{y}$, of the crosshead. A theoretical relationship between $\dot{a}$ and $\dot{y}$ may be derived using simple beam theory [5], assuming that the load, P_c, at fracture remains constant for a given TDCB test. Thus, the derivative of the compliance is given by:

$$\dot{C} = \frac{1}{P_c} \cdot \dot{y} \qquad (2)$$

Rearranging Equation (1) using Equation (2) yields:

$$\dot{a} = \frac{P_c}{2bG_c} \cdot \dot{y} \qquad (3)$$

The values of the crack velocity, $\dot{a}$, versus the applied rate of displacement, $\dot{y}$, of the crosshead from both the experiments and Equation (3) are shown in Figures 6a and b for the aluminium-alloy and the steel joints, respectively. The agreement between the experimental and the theoretical values is relatively good.

In 'Region I' the locus of joint failure was always visually interfacial between the adhesive and the substrate. In Figures 1, 2 and 3, the final point shown for the G_c versus $\dot{a}$ relationships (i.e. at the highest value of $\dot{a}$) for 'Region I' behaviour represents the fastest crack velocity that could be recorded. Indeed, increasing the rate of displacement of the test above this value by a small increment led to the observation of 'Region II' or 'Region III' behaviour.

As may be seen from the data shown in Figures 1 to 3 and as discussed below, the exact values of crack velocity corresponding to these three regions is dependent upon the substrate and surface pretreatment employed, and the test environment. However, as an approximate guide, 'Region I' encompasses the crack velocity range from about 10^{-3} to 10mm/min.

3.3 'Region III' Behaviour

'Region III' behaviour was observed at relatively high rates of displacement, $\dot{y}$. Here the crack grew in an unstable, stick-slip manner with the crack growing in an uncontrolled way, at a relatively fast velocity, and then arresting. These observations are clearly in direct contrast to the

results from ‘Region I’. Furthermore, unlike that observed in ‘Region I’, the locus of joint failure in ‘Region III’ was always essentially cohesive through the adhesive layer.

This type of unstable crack growth has a significant effect on the associated load, P, versus displacement, y, curve which now had a characteristic saw-tooth appearance, as may be seen from Figure 7. The peak values of the load, P_c, represent the value of the load for the onset of crack growth and the average of these values was used to determine the value of the adhesive fracture energy, G_c, as indicated above. The values of G_c obtained are of the order expected for this type of adhesive [15]. When unstable crack growth was observed, the crack propagated at a relatively high velocity, which was too high to be measured using the video camera. However, an approximate value of the crack velocity was estimated from previously published data by Gledhill and Kinloch [16]. They applied a grid of conductive paint to the side of the TDCB specimen and, via the change in electrical resistance of the grid as the crack propagated and ruptured the paint grid, obtained the relationship between G_c and $\dot{a}$ for a similar adhesive system which exhibited unstable crack growth. Using the data of Gledhill and Kinloch, the crack velocity corresponding to the G_c value in ‘Region III’ for the present tests was about 20 km/minute for both the ‘GBD’- and ‘GBS’-pretreated joints. This value was therefore taken to represent the resulting crack velocity for unstable crack growth in the present studies. This is obviously an approximation, but the absolute value of the crack velocity associated with the unstable crack growth ‘Region III’ has no significant effect on the interpretation of the results obtained in the present study.

Finally, it is noteworthy that Arnott and Kindermann [17] have also studied the effect of a constant rate of displacement on the value of G_c of structural joints. Although they did observe in their experiments what we have termed ‘Region III’ behaviour, such cohesive in the adhesive failure was still associated with stable crack growth

3.4 'Region II' Behaviour

'Region II' is a transition region between 'Region I' and 'Region III'. Two sub-types of 'Region II' were identified as explained below, denoted as 'Region IIa' and 'Region IIb' respectively. (For reasons of clarity, the specific 'Region II' has in some instances been omitted from Figures 1 to 3, but the details are given in the text below.)

In the transition region 'Region IIa' experimental data could be obtained for joints where the values of G_c were intermediate between those recorded in 'Region I' and those in 'Region III'. This behaviour may be seen clearly in Figures 1 and 2, as indicated by the 'hatched' areas, for the 'GBD'-pretreated aluminium-alloy and steel joints, respectively. (Indeed, for the aluminium-alloy and steel joints only the 'GBS'-pretreated joints tested in the 55% RH environment did not exhibit 'Region IIa' behaviour.) In 'Region IIa', the locus of joint failure associated with this type of stable crack growth was always visually interfacial between the adhesive and the substrate, as was observed in 'Region I'.

In 'Region IIb' it was not possible to obtain experimental data in the transition region between 'Region I' and 'Region III', as it was for 'Region IIa'. Furthermore, in some instances the increase in the value of G_c on going from 'Region I' to 'Region III' behaviour was relatively low. The regions denoted 'Regions IIb' in Figures 1 and 2 for the 'GBS'-pretreated aluminium-alloy and steel joints, respectively, illustrate both of these aspects for the 'Region IIb' behaviour. Further, the dissimilar joints exhibited 'Region IIb' behaviour under all test conditions, see Figure 3. Thus, the term 'Region IIb' is simply used to represent a change in the type of crack growth, i.e. from stable to stick-slip crack growth, which is always accompanied by a change from visually interfacial to cohesive in the adhesive failure, as the rate of displacement, $\dot{y}$, is steadily increased.

3.5 Effect of Substrate

As noted above, the results for the values of G_c as a function of corresponding crack velocity, $\dot{a}$, are shown for various types of joints in Figures 1, 2 and 3. There are several interesting points to be seen from these figures.

Firstly, for a given surface pretreatment (i.e. 'GBD' or 'GBS'), when tested at 55% RH, there is no significant effect of choice of substrate(s) upon the G_c versus $\dot{a}$ relationship for the different types of joint, and this statement applies to the results from 'Region I', 'Region II' and 'Region III'. Secondly, for 'Region I' at 55%RH, for both types of surface pretreatment (i.e. 'GBD' and 'GBS'), the value of G_c is almost constant with increasing crack velocity and the slope of the $\log_{10} G_c$ versus $\log_{10} \dot{a}$ relationship in 'Region I' is independent of the type of substrate and surface pretreatment employed. The slope showing a relatively very low dependence of G_c upon the crack velocity, $\dot{a}$, has been found [18] to be controlled by the viscoelastic nature of the epoxy adhesive. Thus, the low dependence of the value of G_c upon the crack velocity was attributed to the low value of the viscoelastic loss factor of the epoxy adhesive in this range, arising from the highly cross-linked structure of the epoxy polymer. However, thirdly, there is a significant effect of the type of substrate(s), and type of joint, in the 'Region I' for the tests conducted in the aqueous environment. This can be discerned from Figures 1 to 3 but is shown more readily when all the types of joint are plotted onto one common graph, see Figures 8a and b for both the 'GBD'- and 'GBS'-pretreated substrates, respectively. Here it may be clearly observed that the joints manufactured using the aluminium-alloy substrates gave the best environmental resistance. On the other hand, joints based on the dissimilar substrates resulted in the joints which were most readily attacked by the aqueous environment. Fourthly, the slope for the relationship between $\log_{10} G_c$ and $\log_{10} \dot{a}$ is far higher in value for the tests undertaken in the aqueous environment than for those conducted in the 55% RH condition. These differences imply

that different mechanisms of environmental attack are operating in the two different test environments.

Turning to 'Region III', when tested in the aqueous environment, the data shows that there are no statistical differences in the values of G_c associated with the various types of joints. The value of G_c in 'Region III' is also independent of the test environment. These observations are to be expected, since in 'Region III' cohesive failure though the adhesive was observed to occur.

3.6 Effect of Surface Pretreatment

The effect of the type of surface pretreatment employed is evident in all three regions of the fracture behaviour of the various types joints, and is of significance for the tests conducted in both test environments, as may been seen from Figures 1, 2, 3 and 8.

In 'Region I', for both test environments, the values of G_c for the 'GBS'-pretreated joints are always clearly higher than for the 'GBD'-pretreated joints based upon the aluminium-alloy, steel and dissimilar substrates. Nevertheless, as commented above, it is noteworthy that the slope of the G_c versus $\dot{a}$ relationship is not affected by the surface pretreatment employed.

In 'Region III', the values of G_c for the 'GBS'-pretreated joints were again somewhat higher than for the 'GBD'-pretreated joints, and this was observed for both the aluminium-alloy and the steel joints, even though the locus of failure was essentially cohesive in the adhesive layer in all cases. The values of G_c, considering both types of substrate, were 1010 J/m^2 ($\pm$100 J/m^2) and 780 J/m^2 ($\pm$100 J/m^2) for the 'GBS'- and 'GBD'-pretreated joints, respectively. (This observation may be explained [18] from work by Maugis [19] who has considered the transition

from stable to stick-slip crack growth that occurs in brittle materials as the crack velocity is increased.)

Finally, considering the onset of 'Region II' behaviour, the maximum velocity that could be sustained in 'Region I' before the transition to 'Region III' behaviour was observed to be far greater for the 'GBD'-pretreated joints than for the 'GBS'-pretreated joints. For instance, for the tests conducted in the 55% RH environment, the maximum velocity measured in 'Region I' for the 'GBD'-pretreated aluminium-alloy joints was 5 mm/minute, whereas for the 'GBS'-pretreated aluminium-alloy joints it was 1 mm/minute. Thus, the transition from 'Region I' to 'Region II' occurred in the 'GBD'-pretreated joints at a significantly higher rate of displacement, and hence crack velocity, than in the 'GBS'-pretreated joints. These observations again reflect the superior durability imparted by the 'GBS' pretreatment, compared to the 'GBD' pretreatment.

4. MECHANISMS OF FAILURE IN 'REGION I'

4.1 The Tests Conducted in 55% RH

4.1.1 Results from Crack Propagation Studies

Before considering the mechanisms in 'Region I' for the tests conducted in 55%RH it is useful to summarise the relevant results from the crack propagation studies reported above. Firstly, it must be emphasised that the interfacial fracture seen in 'Region I' in the 55% RH environment is not intrinsically the result of environmental attack, since joints tested at 0%RH were observed to exhibit 'Region I' behaviour and hence to fail visually along the interface between the adhesive and the substrate [18]. Secondly, however, there is a clear effect of the relative humidity of the test environment in 'Region I': the higher the relative humidity, the lower the adhesive fracture energy, as may be seen in Figure 9. Thirdly, the type of substrate, i.e. whether aluminium-alloy or steel, appears to play no significant role in the degree of environmental attack when a humid environment is employed. However, the choice of surface pretreatment (i.e. 'GBD' versus 'GBS')

and the concentration of water, i.e. the RH, are critical factors. Finally, it is noteworthy that these observations imply that, in 'Region I', the water molecules reach the vicinity of the crack tip at a sufficiently fast rate to enable the environmental attack mechanism to occur readily, since the G_c versus crack velocity dependence is controlled by the viscoelastic nature of the epoxy adhesive, not by the RH employed [18].

4.1.2 The 'GBD'-Pretreated Joints

In the case of the 'GBD'-pretreated joints, the intrinsic stability of the adhesive/substrate interface in the presence of an aqueous environment may be assessed from the thermodynamic arguments advanced by Gledhill and Kinloch [20]. The thermodynamic work of adhesion is defined as the energy required to separate unit area of two phases forming an interface. If only secondary forces (e.g. van der Waals forces) are acting across the interface which is considered to be the main mechanism of adhesion of most epoxy adhesives, then the work of adhesion, W_A, in an inert medium may be expressed by:

$$W_A = \gamma_a + \gamma_s - \gamma_{as} \tag{4}$$

where γ_a and γ_s are the surface free energies of the adhesive and substrate, respectively, and γ_{as} is the interfacial free energy. In the presence of a liquid (denoted by the suffix 'l'), such as water, this expression must be modified and the work of adhesion W_{Al} is now given by:

$$W_{Al} = \gamma_{al} + \gamma_{sl} - \gamma_{as} \tag{5}$$

where γ_{al} and γ_{sl} are the interfacial free energies between the adhesive/liquid and substrate/liquid interfaces, respectively. For an adhesive/substrate interface the work of adhesion, W_A, in an inert

atmosphere, for example dry air, usually has a positive value indicating thermodynamic stability of the interface. However, in the presence of a liquid the thermodynamic work of adhesion, W_{Al}, may well have a negative value indicating that the interface is now unstable and may dissociate. Thus, calculation of the terms W_A and W_{Al} may enable the durability of the interface in the long term to be predicted. The values of W_A and W_{Al} for epoxy/steel joints, respectively, have been reported to be +291 and –255 mJ/m^2 [20]; and for epoxy/aluminium-alloy joints +232 and –137 mJ/m^2 [21]. These values lead to the conclusion that the epoxy/oxide interfaces will indeed be susceptible to attack and degradation upon exposure to water molecules. These ideas have been supported by the use [18] of surface-analytical methods which confirmed that fracture indeed occurred mainly at the interface between the adhesive and the metallic-oxide layer on the substrate. However, it should be borne in mind that the thermodynamic approach describes the behaviour of the joints at equilibrium (i.e. over a relatively long timescale) and, given the short length of the test (i.e. a few hours), it is unlikely that the failure solely occurred as a result of the presence of water molecules. Thus, it is suggested that the joints failed due to both the application of a stress and the presence of water molecules at the crack tip, a phenomenon similar to stress corrosion cracking which occurs in metals and ceramics (see for example [22]). However, as the relative humidity was increased, the number of water molecules was higher and the value of the adhesive fracture energy was seen to decrease, as indeed would be expected.

4.1.3 'GBS'-Pretreated Joints

Silane pretreatments are known to increase the degree of interfacial adhesion, see for example [23-26]. This increase in the intrinsic adhesion has been attributed to the formation of covalent bonds between the metallic substrate and silane primer, and in turn between the silane primer and the adhesive layer; i.e. the silane primer acts as a 'coupling agent'. Indeed, covalent bonds between the substrates and the silane, based upon GPS, have been detected for steel [23, 27] and aluminium [26] using secondary ion-mass spectrometry.

For the present joints tested in 55% RH, the previous studies revealed [18] that the failure occurred mainly in the adhesive layer. However, the XPS spectra suggested that fracture also occurred to a certain extent in the silane and oxide layers. This is presumably due to the asperities on the grit-blasted substrate surface being pulled off during failure, and indicates a complex fracture path. The fact that the failure occurred mainly in the adhesive layer is consistent with the presence of covalent bonds being formed across the adhesive/substrate interface when a silane coupling agent is used, as widely reported in the literature. As for the 'GBD'-pretreated joints, it appears that the 'GBS'-pretreated joints failed as a result of both the application of a stress and the presence of water molecules at the crack tip. And, as the relative humidity was increased, the number of water molecules at the crack tip increased and the adhesive fracture energy decreased as a result; possibly due to the interfacial covalent bonds being attacked and ruptured. Although, for the 'GBS'-pretreated joints, there is a clear suggestion that a critical concentration of water molecules may have to be attained before any such environmental attack occurs [18].

4.2 The Tests Conducted in an Aqueous Environment

4.2.1 Aqueous versus relative humidity tests

The mechanisms of failure have been successfully identified for the joints tested in the 55% RH environment, and indeed at the other levels of relative humidities that were employed. However, clearly, for the joints tested in the aqueous environment then a different mechanism of environmental attack appears to be operative. This is reflected, firstly, in the very different slopes seen in the $\log_{10} G_c$ versus $\log_{10} \dot{a}$ plots for the joints tested in the 55% RH environment, compared to those tested during water immersion, see Figures 1 to 3. Secondly, by further comparing the results from the 100%RH tests to those in water, for example compare Figures 9 and 8a respectively. Thirdly, by the observation that the type of substrate (i.e. employing aluminium-alloy, steel or aluminium-alloy/steel dissimilar substrates) has no effect on the $\log_{10}$

G_c versus $\log_{10} \dot{a}$ relationship for tests conducted in the 55% RH environment, but has a major effect when joints are tested in water, see Figure 8.

4.2.2 Locus of Failure: GBD Joints

As for the 55% RH tests, XPS has been used extensively to assess the exact locus of failure of all joints tested in an aqueous environment. In the case of the aqueous exposure, however, the failure modes are somewhat more complex, particularly in the case of the aluminium-alloy/steel dissimilar-substrates joints. It is therefore necessary to consider the surface analysis in rather more detail, and to achieve this both XPS survey spectra and the quantitative surface analysis derived from their associated high resolution spectra will be considered, for all three types of joint.

In any assessment of the locus of failure it is essential to establish the condition of the surfaces prior to the bonding process. XPS survey spectra for the adhesive and the 'GBD'-pretreated aluminium-alloy and steel surfaces are presented in Figure 10. Both metallic surfaces are relatively very clean for technological surfaces exposed, albeit briefly, to atmospheric conditions. Such exposure gives rise to a small amount of adventitious carbon contamination: approximately 30 atomic % in terms of surface concentration and a thickness of 0.5 to 1.0 nm. The driving force for this contamination is the reduction of surface free energy by the adsorption of a thin layer of carbonaceous material from the air. Such a phenomenon is ubiquitous for a high surface-energy material such as a metal oxide but does not occur to any significant extent with a low surface-energy material, such as a polymeric adhesive. The fate of this material on application of an adhesive is not clear but it is extremely likely that it is either displaced by the adhesive or absorbed into it. However, one aspect is clear: it does not remain at the junction between metal substrate and adhesive as it would form a weak boundary layer which would compromise joint performance. It does, however, present a slight problem in the interpretation of

the locus of failure data in that a low level of carbon on an interfacial metal failure surface might be either the result of (a) a true interfacial failure which has subsequently adsorbed carbon from the atmosphere or (b) a locus of failure in which the fracture path has passed very close to the interface but left a very thin layer of adhesive on the metal substrate. In order to resolve this dilemma we need to consider the spectrum of Figure 10 (a) of the epoxy adhesive. The N1s signal (ca. 400 eV) is clearly seen and equates to a surface concentration of nitrogen of 3.2 atomic %, thus in order to define the locus of failure exactly we need to consider not only the total assay of carbon on the metal failure surface but also the surface concentration of nitrogen from the amine curing agent.

Turning now to the adhesive joints themselves, it is helpful to consider the steel/steel and aluminium-alloy/aluminium-alloy joints before moving on to the aluminium-alloy/steel joints. XPS survey spectra for the interfacial metal failure surfaces of the similar substrate joints are presented in Figure 11. Both these spectra show a modest amount of carbon, as may be seen from the quantitative XPS data of all interfacial failure surfaces in Table 4, but at levels that are slightly higher than the unbonded controls, indicating that there is a small amount of adhesive residues on the metal surface, although the failure mode is predominantly interfacial. This conclusion is reinforced by relatively low, but significant concentrations of nitrogen (i.e. 1.4 and 1.3 atomic % for aluminium-alloy and steel substrates, respectively) associated with the metal failure surface. Although the spectra are not shown, the quantitative date from the adhesive failure surfaces are also included in Table 4. Both adhesive surfaces show a small concentration (i.e 0.6 atomic % Al, 1.8 atomic % Fe) of metal transferred to the adhesive side of the failure. In the case of the aluminium-alloy surface it is most likely to be a result of the fracture of asperities of the grit-blasted surfaces, as discussed above for specimens tests at 55% RH.

The situation for the steel/steel substrate joints is rather different and the presence of iron on the adhesive is thought to be a result of the back-deposition of corrosion products which occur as a post-failure event. This hypothesis is reinforced by the visual appearance of the adhesive side of the beam which has a faint brown (rust) colouration at the outermost edges. The alternative explanation, that there is failure occurring in the oxide or corrosion product itself, is possible but given the thin layer of oxide present on the steel to start with, and the electrochemical reactions that occur at the crack tip which will be considered in the next section, this is unlikely. There is a small amount of Al on both the adhesive and steel-substrate failure surfaces which is thought to arise from embedded alumina grit. Given this observation, it is quite reasonable to ascribe the modest Al signal on the adhesive side of the failed aluminium-alloy joint to the same source, although asperity fracture is still a plausible alternative.

In summary, the loci of failure for both 'GBD'-pretreated steel and aluminium-alloy joints is predominantly along the interface with small amounts of cohesive failure in the adhesive and the respective metal oxides. The adhesive surface from the steel/steel joint is decorated with iron corrosion product. However, in the case of the aluminium-alloy/aluminium-alloy joint, the passive film protecting the metallic alloy ensures general corrosion does not occur, although any corrosion present on this substrate will take the form of pitting at inclusions and/or grain boundary triple-points.

Turning now to the steel/aluminium-alloy dissimilar-substrate joints, these joints always failed at the adhesive/steel interface and the spectra from both the metal and the adhesive interfacial surface are shown in Figure 12. The quantitative data from these spectra are also included in Table 4. The spectrum of the steel substrate, see Figure 12a, is very similar to the metal failure surface of the steel/steel substrate joint shown in Figure 11b. The significant differences are the slight increases in carbon and nitrogen, indicative of slightly more adhesive

residues at the steel failure surface of the dissimilar joint compared with the steel/steel assembly. The concentration of calcium at the surface is comparable to the aluminium-alloy/aluminium-alloy joint, but increased somewhat relative to the steel/steel joint.

It is the calcium marker ions, present on all the metal failure surfaces, that provide a clue to the mechanism of failure, indicating that electrochemical activity is responsible for the enhanced failure in water compared to 55%RH. The adhesive surface is spectroscopically similar to that of the steel/steel joint, although the surface concentration of carbon is significantly higher with a concomitant decrease in the iron signal. Once again, these iron residues are believed to be back-deposition of iron corrosion species following the anodic dissolution of the substrate in the environs of the crack tip, or general corrosion of the steel beam in the aqueous medium.

4.2.3 The Role of Corrosion

The steel/steel and the steel/aluminium-alloy joints both showed evidence of corrosion on all steel beams. At this point it is worth reviewing the corrosion process with a view to assessing its role in the current failure process. The corrosion of iron can be considered in terms of the two relevant electrode half reactions: at the anode anodic dissolution of iron occur whilst at the cathode water and oxygen are reduced to hydroxide ions:

Anode: $Fe \rightarrow Fe^{2+} + 2e^-$

Cathode: $2H_2O + O_2 + 4e^- \rightarrow 2OH^-$

The anodic product is Fe(II) ions which are soluble, and on oxidation are converted to Fe(III) ions which are insoluble and will deposit on a nearby surface. It is the hydroxide ions, produced by the reduction of water and oxygen molecules, that are deleterious to adhesion. In the

case of metal surfaces covered with an organic coating or adhesive, the two electrode half reactions occur at discrete sites, the cathodic process occurring at the tip of an advancing crevice. This phenomenon is known as cathodic delamination (or disbondment) and has been well documented for structural adhesives [27] as well as organic coatings [28, 29]. In the case of the steel/steel joints it is clear that the major mechanism responsible for failure is cathodic delamination, as indicated in Figure 13. In the case of the aluminium-alloy/aluminium-alloy joint the passive film present on the substrate surface reduces the extent of corrosion quite dramatically. However, it is clear that a cathodic delamination process plays a small part in the failure mechanism, perhaps by creating a small crevice which allows the ingress of liquid water, the usual hydrodynamic displacement process will then come into play.

At this point it is useful to justify the use of calcium, and other cations, as markers for cathodic activity when the anode and cathode are separated as discrete electrode sites. At the cathodic surface hydroxide ions are produced as described by the cathodic half-reaction above. In order to achieve charge balancing, cations, in the environs of the cathodic surface, are adsorbed onto the surface, which achieves electrical neutrality. In the case of an electrochemical test using 3% NaCl, or a similar electrolyte, a significant Na1s signal is seen in the XPS spectrum of these surfaces exposed to cathodic polarisation whilst those which have experienced anodic conditions will show an excess of anions (Cl^-) [30]. For adhesive joints tested in pure water the ions deposited are those present at very low concentrations, typically calcium, and it has been shown [27] that the surface concentrations of Ca^{2+} deposited can be very low, at the detection limit of XPS. Thus, from these studies, the use of SIMS was recommended to be employed, with its better detection limit, to assay such a marker ion when the test is carried out in pure water.

Having established the role of corrosion in the steel/steel joint it becomes apparent that such a phenomenon is important in the case of the dissimilar substrates joint. At first sight the

occurrence of the failure at the steel/adhesive interface would seem to be a simple case of galvanic corrosion, as an aluminium-alloy will be at the more active end of the galvanic series than steel. For such galvanic coupling to occur there needs to be electrical contact between the aluminium-alloy and steel substrates. This is not thought to occur and a separate set of experiments using 'Tufnol' pins in the testing machine, and insulating spacer wires in the adhesive layer, to ensure that there was not electrical contact between steel and aluminium-alloy beams, produced the same fracture and interfacial chemistry results. Also, it should also be noted that corrosion occurred on the steel beam which would not be present had the steel beam been the cathodic part, in its entirety, of a galvanic cell. Now, the reason for the inferior durability of the dissimilar joints is thought to lie in the diffusion of oxygen molecules into a developing crevice and the concomitant outward diffusion of the cathodic reaction product (OH^-). It is helpful at this point to consider the situation in terms of oxygen supply that exists for the steel/steel joint. Along the sides of both beams the anodic reaction will take place and soluble Fe(II) ions will pass into the solution leading to a local increase in density. Thus, this solution of water and Fe(II) ions will sink to the bottom of the testing tank and the solution in the environs of the adhesive layer will be refreshed with aerated water. This situation ensures that there is a ready supply of reactants for the cathodic reaction which develops a crevice ***normal*** to the direction of crack propagation (i.e. the length of the test piece). As the diffusion of hydroxyl ions is known to be rapid in aqueous solution it is likely that the aggregation of these species at the crack tip is modest, in other words the diffusion coefficient of water molecules into the crevice is much the same as that of hydroxide ions diffusing outwards. Thus, the rate controlling step may be taken to be the rate of arrival of the water molecules which must feed the two developing cathodic crevices. This situation is illustrated schematically in Figure 14. In the case of the aluminium-alloy/steel joint the two metal interfaces will not behave in the same manner, the steel adhesive interface will develop a cathodic crevice as described above but, as the aluminium-alloy has a passivated film present, the extent of cathodic reactions at this surface will be confined to regions surrounding localised corrosion such

as pitting on the failure surface of the beam. That is to say any corrosion on the aluminium-alloy beam will be a post-failure event. This means that the majority of the oxygen molecules dissolved in the aqueous bath adjacent to the adhesive layer are available for consumption by the cathodic half reaction at the steel/adhesive interface. Assuming the outward diffusion of hydroxide ions remains the same, the situation that now exits is that the inward diffusion of oxygen molecules exceeds the outward diffusion of hydroxide ions. This will lead to an aggregation of hydroxide ions at the crevice tip and an increase in pH in this region. This will have an increased damaging effect on the level of adhesion between adhesive and steel substrate and the associated reduction in performance. The adhesive side of the failure shows, once again signs of discolouration at the outermost edge, as shown schematically in Figure 15 (a), which represents a short section from the mid-region of the beam. This is thought to be corrosion deposit and XPS analysis within this region at a 50 μm spot size confirms the visual interpretation, as indicated in the montage of Fe2p spectra taken from across the failure surfaces of both sides of the failed joint, Figure 15.

To summarise, the situations are as expected for the same substrate joints whilst for the aluminium-alloy/steel joint the increased concentration of oxygen molecules available in solution to feed the crevice developing normal to the beam side at the steel/adhesive interface weakens the joint and leads to more rapid advancement of the crack tip, see Figure 8a. As the crevice develops so the crevice mouth becomes anodic and the corrosion product is back-deposited reducing the inward diffusion of water and oxygen molecules. However, by this time the damage is already done and the mechanical perturbation of the reduced area at the advancing crack tip has brought about failure. The development of the cathodic crevice happens along the beam simultaneously. Thus, the effect is most serious in the mid-regions where the crevice has developed significantly but not been blocked by corrosion product. The situation is summarised schematically in Figure 16.

4.2.4 The Effect of Surface Pretreatment

So far only the 'GBD'-pretreated joints have been considered. In this section the mechanisms of failure and the role of electrochemical activity on the 'GBS'-pretreated joints will be considered. The XPS survey spectra from 'GBS'-pretreated aluminium-alloy and steel surfaces are presented in Figure 17 and the associated quantitative surface analysis for theses surfaces and the interfacial failure surfaces are given in Table 5.

The data from the 'GBS'-pretreated surfaces are superficially very similar to that from the 'GBD' joints, but there are small but significant concentrations of Si (i.e. 2.5 at% on the aluminium-alloy surface, 3.5 at% on the steel surface). This arises from the silane treatment involved and indicates the deposition/incorporation of the GPS at the metal surface. The presence of a covalent bond between the silanol of hydrolysed organosilane and metal surfaces is the well established mode of operation responsible for the improvement of the durability of adhesive joints using these adhesion promoters and such a bond is readily identified using SIMS [23, 26]. In the case of an aluminium-alloy a fragment ion is seen at a nominal mass of 71 ($SiOAl^+$) whilst for the steel substrate a fragment at 100 will be observed ($FeOSi^+$). Positive ToF-SIMS data recorded from 'GBD'- and 'GBS'-pretreated aluminium-alloy and steel surfaces are presented in Figures 18 and 19, respectively. Although recorded at relatively low spectral resolution for a ToF-SIMS system, the presence of both candidate fragments is clearly seen for the 'GBS'-pretreated surfaces and is absent for the 'GBD'-pretreated substrates.

The low mass range m/z = 24-34 has also been included from the 'GBS'-pretreated aluminium-alloy surface and the development of the Si^{28} ion is seen along with the adjacent Al^{27} cation. Thus any comparison between the failure mechanism of 'GBD'- and 'GBS'-pretreated joints must take into account the different adhesion mechanisms: in the case of a 'GBD'-pretreated joint the interfacial adhesion will arise from solely on secondary forces such as

dispersion, polar and hydrogen bonding forces, and specific interactions such as acid-base bonding; whilst for ‘GBS’-pretreated joints it will also involve primary (covalent) bonding between the silane adhesion-promoter and the metallic substrate, and also the adhesion promoter and adhesive [31].

XPS survey spectra of the metal interfacial failure surfaces are shown in Figure 20 and, although broadly similar to comparable spectra from ‘GBD’-pretreated substrates, they show two significant differences, for both the aluminium-alloy and the steel substrates the carbon and nitrogen concentrations are all increased slightly indicating an increased amount of cohesive failure within the adhesive itself, see Table 5. The silicon concentrations are consistent on all interfacial failure surfaces of the same metal joints at around 0.8 at%. On the ‘GBD’ joints, the Si concentration varied from below the detection limit of XPS ca. 0.05 at% to >1 at%. The consistency on the ‘GBS’-pretreated joints when taken with the Si concentration on the unbonded ‘GBS’ surfaces indicates that there is some failure in the organosilane rich layer. In the case of the dissimilar substrate joints there are similarities with both the dissimilar joints manufactured from the ‘GBD’-pretreated substrates and the steel ‘GBS’-pretreated joints, discussed above. The occurrence of the locus of failure close to the steel/adhesive interface indicates the same overall failure mechanism is at work as was seen for the ‘GBD’ joints. There is a surplus of oxygen available at this interface which leads to the development of a cathodic crevice and associated weakening of the joint at this point. The presence of a degree of covalent bonding, however, ensures that the joint is more durable than the simple ‘GBD’ pretreatment. The development of an alkaline environment will still be deleterious to the level of adhesion achieved, although the effect will not be so pronounced as in the case of simple dispersion or acid-base bonds. The presence of a small (i.e. <1 at%) assay of silicon on all adhesive interfacial failure surfaces indicates that some failure occurs at the interphase region between silane and metallic substrate. However, as there is silicon on both the steel (3.5 at%) and aluminium-alloy (2.5 at%) ‘GBS’-pretreated

surfaces, it is clear that there is no failure between the adhesive and outer surface of the silane pretreatment layer to any significant extent.

In summary, the application of the 'GBS'-pretreatment to aluminium-alloy and steel substrates leads to the development of a degree of covalent bonding, as predicted in the literature. This enhances the durability of these joints and when failure does occur is of a complex mixed mode type, with a significant proportion occurring at the interface between the silane layer and the metallic substrate.

5. CONCLUSIONS

The adhesive fracture energy, G_c, of metallic joints, bonded with a rubber-toughened epoxy adhesive, has been measured using monotonically-loaded tests. Such tests have been conducted in various relative humidities and in water, at 21^{o}C. Two surface pretreatments have been employed for the substrates prior to bonding: a simple grit-blast and degrease ('GBD') pretreatment or a silane primer ('GBS') pretreatment. The joints were formed using metallic substrates which were either (a) aluminium-alloy substrates, (b) steel substrates, or (c) 'dissimilar' substrates (i.e. one substrate being aluminium-alloy with the other one being steel). For both test environments, when G_c was plotted against the crack velocity, three regions of fracture behaviour could be distinguished. At low rates of displacement the crack grew in a stable manner, visually along the interface, and relatively low crack velocities could be readily measured. This was considered to be the most important region and was termed 'Region I'. Here the value of G_c measured in the aqueous environment was relatively low compared to that measured in a relatively dry environment of 55% relative humidity.

The loci of joint failure have been studied using surface-specific analytical techniques. There are several potential loci of failure that can occur in the fracture of adhesive joints ranging, on the one hand, from true interfacial separation along the adhesive/substrate interface to a cohesive failure in the adhesive, or unusually the substrate. In the work described in the present paper a variety of loci of failure have been identified, using XPS, and the associated mechanisms of environmental failure identified for the joints which failed in 'Region I'.

For the tests conducted at 55% RH, the failure mode is critically dependent on the substrate pretreatment, but not on the type of substrate(s) employed. In the case of the 'GBD'-pretreated substrates water condenses at the developing crack tip and stress-assisted interfacial separation occurs. This is essentially a hydrodynamic process and can be readily predicted using a thermodynamics approach. In the case of the 'GBS' pretreatment, the interface is much more durable, since interfacial covalent bonds are formed and resist such hydrodynamic attack. Thus, the locus of joint failure is predominantly associated with cohesive failure in the adhesive.

For the joints tested in liquid water the type surface pretreatment and the type of substrate employed were both of importance. Here a corrosion process is seen to play a role in failure, and a cathodic disbondment mechanism occurs, once again leading to a predominantly interfacial failure, although the kinetics will be faster than the simple hydrodynamic displacement described above. In the case of the dissimilar-substrate joints, failure always occurs at the steel/adhesive interface, which is a result of the greater cathodic activity in the crevice associated with this interface. The supply of oxygen to this crevice is the rate-controlling step in the production of hydroxide ions. The use of the silane adhesion-promoter in the 'GBS' pretreatment again enhances the level of durability of the adhesive/substrate interface, but this region of the joint is still relatively vulnerable to environmental attack. Unlike the 55 %RH specimens, where the failure is seen to move into the adhesive, the failure of the joints exposed to water still occurs

predominantly in the interphase region with evidence that a significant proportion of the failure now occurs at the silane/substrate boundary.

Acknowledgements

The authors would like to thank Dr. D. Tod (QinetiQ) for financial support. They also wish to thank Mr. Steve Greaves of the University of Surrey for conducting the XPS studies and Professor Jim Castle for invaluable discussions regarding corrosion phenomena.

References

1. A. J. Kinloch, (Ed.), "Durability of Structural Adhesives" (Applied Science Publishers, London, 1983).
2. A. J. Kinloch, "Adhesion and Adhesives: Science and Technology" (Chapman and Hall, London, 1987).
3. A. J. Kinloch, *Proc. Instn. Mech. Engrs*. **211** Part G (1997) 307.
4. R. P. Digby and S. J. Shaw, *Int. J. Adhesion and Adhesives* **18** (1998) 261.
5. B. R. K. Blackman, H. Hadavinia, A. J. Kinloch, M. Paraschi and J. G. Williams, *Eng. Fract. Mech*. **70** (2003) 233.
6. F. E .M. O'Brien, *J. Scientific Instruments* **25** (1948) 73.
7. S. M. Wiederhorn, *J. Am. Ceram. Soc.* **50** (1967) 407.
8. D. R. Arnott and M. R. Kindermann, *J. Adhesion* **48** (1995) 101.
9. C.K. Gurumurthy. E.J. Kramer and C.Y. Hui, *Int. J. Fract.* **109** (2001) 1.
10. M.W. Lane, J.M. Snodgrass and R.H. Dauskardt, *Microelectronics Reliability*, **41** (2001) 1615.
11. J.M. Snodgrass, D. Pantelidis, M.L. Jenkins, J.C. Bravman and R.H. Dauskardt, *Acta Materialia* 50 (2002) 2395.
12. S.Y. Kook and R.H. Dauskardt, *J. Applied Physics* **91** (2002) 1293.
13. S. Strohband and R.H. Dauskardt, *Interface Sci*. **11** (2003), 11.
14. C.K. Gurumurthy. E.J. Kramer and C.Y. Hui, *J. Adhesion* **82** (2006) 239.
15. A. J. Curley, H. Hadavinia, A. J. Kinloch and A. C. Taylor, *Int. J. Fract.* **103** (2000) 41.
16. R. A. Gledhill and A. J. Kinloch, *J. Materials Sci. Letters* **10** (1975) 1261.
17. D. R. Arnott and M. R. Kindermann, *J. Adhesion* **48** (1995) 85.
18. C. F. Korenberg, A. J. Kinloch and J. F. Watts, *J. Adhesion* **80** (2005) 169.
19. D. Maugis, *J. Materials Sci.* **20** (1980) 3041.
20. R. A. Gledhill and A. J. Kinloch, *J. Adhesion* **6** (1974) 315.
21. A. J. Kinloch, W. A. Dukes and R. A. Gledhill, "Adhesion Science and Technology, **9B**" (Plenum Press, New York, 1975) 597.
22. J. Yahalom and A. Aladjem (Eds.), "Stress Corrosion Cracking" (Freund, Tel Aviv, 1980).
23. M. Gettings and A. J. Kinloch, *J. Materials Sci*. **12** (1977) 2511.
24. E. P. Plueddeman (Ed.), "Silane Coupling Agents" (Plenum Press, New York, 1982).
25. S. J. Davis and J. F. Watts, *Int. J. Adhesion and Adhesives* **16** (1996) 5.
26. M.-L. Abel, R. P. Digby, I. W. Fletcher and J. F. Watts, *Surface and Interface Analysis* **29** (2000) 115.
27. S. J. Davis and J. F. Watts, *J. Mater. Chem.* **6** (1996) 479.
28. J. F. Watts and J. E. Castle, *J. Materials Sci.* **18** (1983) 2987.
29. H. Lediheiser. *J. Adhes. Sci. Tech.* **1** (1987) 79.

30. J. E. Castle and D. C. Epler, *Surface Sci.* **53** (1975) 286.
31. A. Rattana, J. D. Hermes, M.-L. Abel and J. F. Watts, *Int. J. Adhesion and Adhesives* **22** (2002) 205.

Table 1 Chemical composition of BS 970 070M55 steel (by weight).

C	Mn	Si	S	P	Fe
0.5-0.6 %	0.5-0.8%	0.15-0.35%	0.04% max	0.04% max	balance

Table 2 Chemical composition of BS 7075 aluminium-alloy (by weight).

Zn	Mg	Cu	Cr	Fe	Si	Ti	Al
5.1-6.1 %	2.1-2.8%	1.2-2.0%	0.18-0.4%	0.7% max	0.50% max	0.20% max	balance

Table 3 **Expected and measured relative humidities (RHs) obtained from using the saturated salt solutions at 21±1°C.**

Saturated salt solution	Expected RH	Measured RH
$CaHPO_4.2H_2O$	95%	96-98%
Na_2SO_4	93%	88-94%
$(NH_4)_2SO_4$	81%	78%
$NaNO_2$	66%	58-72%
KNO_2	45%	48-50%
$CaCl_2$	32%	36-38%
CH_3COOH	20%	19-22%
$ZnCl_2$	10%	10-13%
P_2O_5	0%	1-5%

Table 4. Quantitative XPS surface analyses of interfacial failure surfaces of GBD pretreated joints tested in water.

Joint Type		Surface Composition/atomic %										
		C	O	Al	Fe	N	Ca	Cl	Na	Mg	Si	Zn
GBD Al Alloy Substrate		28.8	51.0	14.4	-	0.7	0.8	-	2.3	1.5	-	0.5
GBD Steel Substrate		30.8	50.5	6.7	6.8	0.6	-	0.2	4.4	-	-	-
Adhesive Control		79.0	16.8	-	-	3.1	-	0.3	-	-	0.8	-
Al Alloy	Metal failure surface	38.4	44.6	12.4	0.4	1.4	0.7	-	-	0.8	1.3	-
	Adhesive failure surface	74.2	20.3	0.6	-	3.3	0.8	0.2	0.6	-	-	-
Steel	Metal failure surface	33.0	56.0	3.6	5.9	1.3	0.2	-	-	-	-	-
	Adhesive failure surface	55.5	33.3	1.8	2.4	3.6	-	0.2	-	-	3.2	-
Dissimilar Substrates	Metal failure surface	44.8	41.6	1.6	7.9	2.0	0.7	-	-	-	1.4	-
	Adhesive failure surface	71.2	22.8	0.6	1.3	3.4	0.3	0.1	-	-	0.3	-

Table 5. Quantitative XPS surface analyses of interfacial failure surfaces of GBS pretreated joints tested in water.

Joint Type		Surface Composition/atomic %										
		C	O	Al	Fe	N	Ca	Cl	Na	Mg	Si	Zn
GBS Al Alloy Substrate		33.7	47.2	12.9	-	1.8	0.4	-	0.7	0.8	2.5	-
GBS Steel Substrate		41.3	44.4	4.2	3.6	2.1	0.1	-	0.5	0.3	3.5	-
Adhesive Control		79.0	16.8	-	-	3.1	-	0.3	-	-	0.8	-
Al Alloy	Metal failure surface	51.8	34.6	8.7	-	2.5	1.2	-	0.4	0.5	0.4	-
	Adhesive failure surface	69.2	23.9	1.1	-	3.8	0.3	0.2	-	0.6	0.8	-
Steel	Metal failure surface	44.1	44.6	4.2	3.9	1.1	0.5	-	-	0.7	0.8	-
	Adhesive failure surface	71.2	24.0	0.4	-	2.9	0.2	0.2	0.1	0.1	0.8	-
Dissimilar Substrates	Metal failure surface	47.8	43.0	2.7	1.9	2.5	0.7	-	0.4	0.3	0.8	-
	Adhesive failure surface	66.4	27.1	0.9	0.6	3.9	0.4	0.2	-	-	0.4	-

LIST OF FIGURE CAPTIONS

FIGURE 1 Relationship between the fracture energy, G_c, and the crack velocity, $\dot{a}$, for the 'GBD'- and 'GBS'-pretreated aluminium-alloy joints. Results are shown for tests conducted at both 21±1°C at 55% RH and in water. (In these figures the solid or dashed lines ending with an arrowhead indicate that no results could be obtained in this range, since the type of crack growth changed from stable to unstable, as discussed in the text.)

FIGURE 2 Relationship between the fracture energy, G_c, and the crack velocity, $\dot{a}$, for the 'GBD'- and 'GBS'-pretreated steel joints. Results are shown for tests conducted both at 21±1°C at 55% RH and in water. (In these figures the solid or dashed lines ending with an arrowhead indicate that no results could be obtained in this range, since the type of crack growth changed from stable to unstable, as discussed in the text.)

FIGURE 3 Relationship between the fracture energy, G_c, and the crack velocity, $\dot{a}$, for the 'GBD'- and 'GBS'-pretreated aluminium-alloy/steel dissimilar joints. Results are shown for tests conducted both at 21±1°C at 55% RH and in water. (In these figures the solid or dashed lines ending with an arrowhead indicate that no results could be obtained in this range, since the type of crack growth changed from stable to unstable, as discussed in the text.)

.

FIGURE 4 Typical load, P, versus displacement, y, curve associated with stable crack growth, as seen in 'Region I' (and 'Region II'). The specimen was a 'GBD'-pretreated steel joint tested at 0.1 mm/minute at 55%RH.

FIGURE 5 Relationship between crack length, a, and time, t, as seen in 'Region I'. The specimen was a 'GBD'-pretreated steel joint tested at 0.05 mm/minute at 55%RH.

FIGURE 6 Relationship between crack velocity, $\dot{a}$, and rate of displacement, $\dot{y}$, as seen in 'Region I' for the 'GBD'-pretreated (a) aluminium-alloy joints and (b) steel joints. (For each type of substrate: ♦: experimental points; and x: points given by Equation (3). The straight line plotted represents the best statistical fit for the experimental data, as obtained via a linear regression analysis.)

FIGURE 7 Typical load, P, versus displacement, y, curve associated with stick-slip crack growth, as seen in 'Region III'. The peaks correspond to crack initiation and the valleys to crack arrest. The specimen was a 'GBS'-pretreated aluminium-alloy joint tested at 0.1 mm/minute at 55%RH.

FIGURE 8 Relationship between the fracture energy, G_c, and the crack velocity, $\dot{a}$, for the (a) 'GBD'- and (b) 'GBS'-pretreated joints in 'Region I' for the tests conducted in the water.

FIGURE 9 Relationship between the fracture energy, G_c, and the crack velocity, $\dot{a}$, for the 'GBD'-pretreated aluminium-alloy joints obtained at 0%, 55% and 100%RH. (Filled circles: 0%RH; open circles: 55%RH and open diamonds: 100%RH.)

FIGURE 10 XPS survey spectra for "control" surfaces: (a) adhesive, (b) 'GBD'-pretreated aluminium-alloy, (c) 'GBD'-pretreated steel.

FIGURE 11 XPS survey spectra of the interfacial metal failure surfaces for similar substrate joints tested in water: (a) 'GBD'-pretreated aluminium-alloy, (b) 'GBD'-pretreated steel.

FIGURE 12 XPS survey spectra of the failure surfaces from the 'GBD'-pretreated dissimilar substrate joint tested in water: (a) the steel failure surface, (b) the adhesive failure surface.

FIGURE 13 Schematic representation of the cathodic disbondment mechanism that is responsible for failure when joints are exposed to liquid water. The cathodic reduction of water at the crack tip produces hydroxide ions which leads to adhesion loss at the interface. Electrons required for this reaction must first be produced at the adjacent anodic site where metal dissolution occurs.

FIGURE 14 Schematic illustration of the supply of oxygen ($\boldsymbol{J_{O2}}$) to the crevice(s) developing at the adhesive-layer/substrate interface(s). As freshly aerated water arrives so it must supply oxygen to both crevices in the case of the steel/steel joint but only the steel/adhesive interface in the case of the dissimilar substrate joint.

FIGURE 15 Evidence for iron residues on the adhesive side of the failed 'GBD'-pretreated steel joint: (a) Schematic appearance of adhesive failure surface at midpoint along the length of the TDCB specimen, showing positions for XPS analysis. (b) Fe2p XPS spectra from the regions of (a) showing the presence of iron near the edge of the specimen. (c) Complementary Fe2p spectra from equivalent positions on the steel side of the joint.

FIGURE 16 Schematic representation of the factors influencing supply of oxygen in the developing crevices. (a) in the early stages of failure oxygen is supplied at the advancing crevice tip as the crack proceeds along the length of the beam and also normal to the direction of crack growth to establish a small but significant developing crevice at the edge of the specimen. (b) the edge crevice may become blocked with corrosion products in this manner in the later stages of joint failure and thus have a disproportionate effect on the failure kinetics.

FIGURE 17 XPS survey spectra for the silane pretreated substrates: (a) 'GBS'-pretreated aluminium-alloy, (b) 'GBS'-pretreated steel.

FIGURE 18 Positive ToF-SIMS spectra for aluminium-alloy substrate: (a) m/z = 60 – 80 for 'GBD' pretreatment, (b) m/z = 60 – 80 for 'GBS' pretreatment, the arrowed peak at m/z = 71 is assigned to $SiOAl^+$, (c) m/z = 24 -34 for 'GBS' pretreatment, the peak at m/z = 27 is Al^+.

FIGURE 19 Positive ToF-SIMS spectra in the mass range m/z = 90 – 106 for the 'control' steel substrates: (a) a 'GBD' pretreatment, (b) a 'GBS' pretreatment, the arrowed peak at m/z = 100 is assigned to $FeOSi^+$.

FIGURE 20 XPS survey spectra of the interfacial metal failure surfaces for the silane treated similar substrate joints tested in water. (a) 'GBS'-pretreated aluminium-alloy, (b) 'GBS'-pretreated steel.

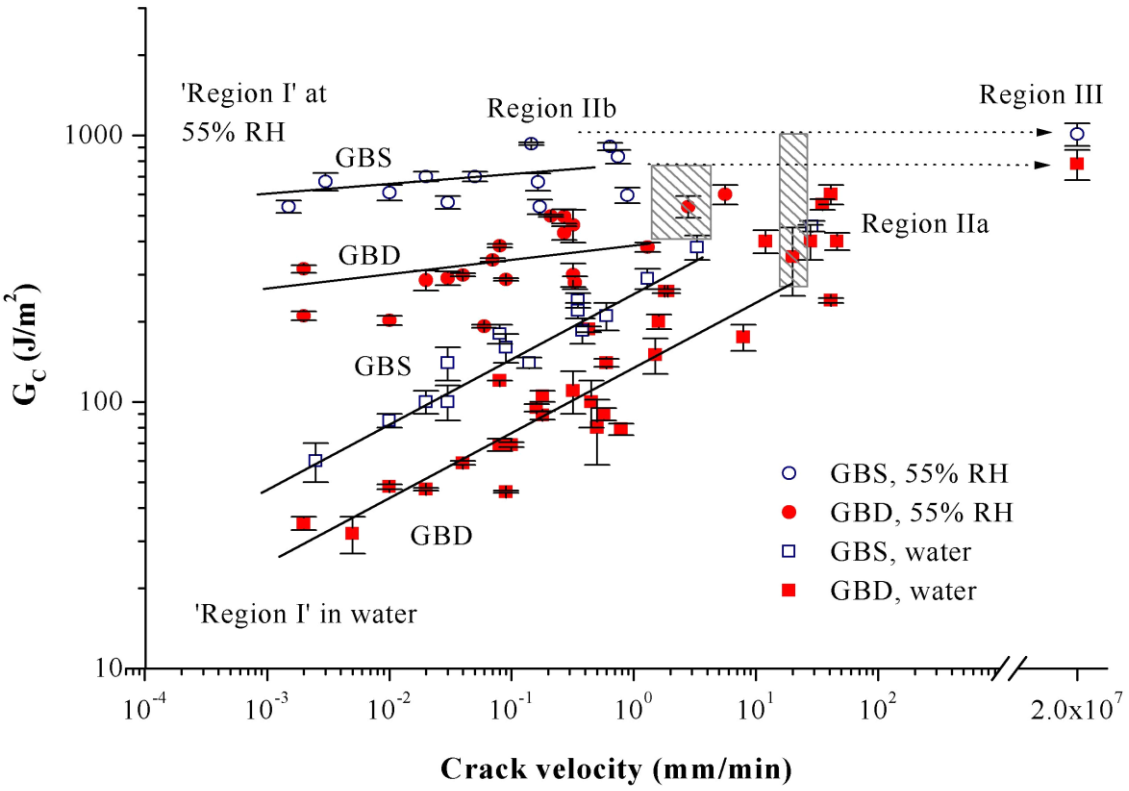

FIGURE 1 Relationship between the fracture energy, G_c, and the crack velocity, $\dot{a}$, for the 'GBD'- and 'GBS'-pretreated aluminium-alloy joints. Results are shown for tests conducted at both 21±1°C at 55% RH and in water. (In these figures the solid or dashed lines ending with an arrowhead indicate that no results could be obtained in this range, since the type of crack growth changed from stable to unstable, as discussed in the text.)

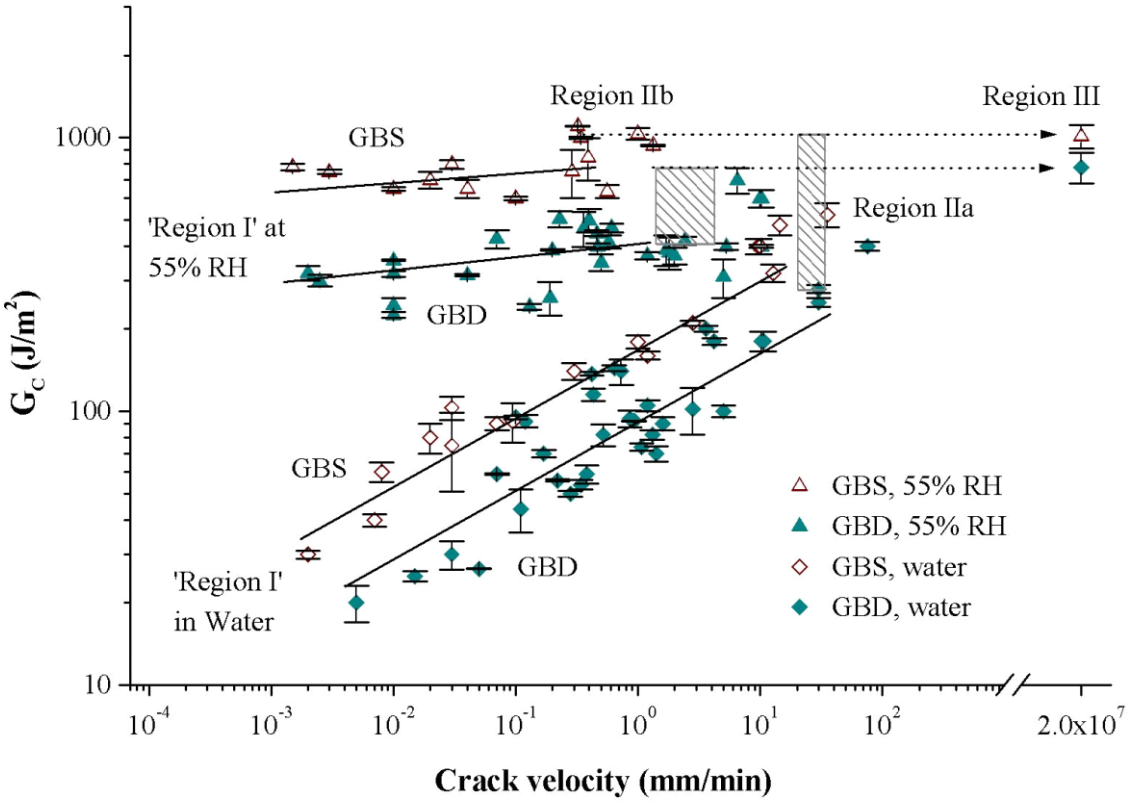

FIGURE 2 Relationship between the fracture energy, G_c, and the crack velocity, $\dot{a}$, for the 'GBD'- and 'GBS'-pretreated steel joints. Results are shown for tests conducted both at 21±1°C at 55% RH and in water. (In these figures the solid or dashed lines ending with an arrowhead indicate that no results could be obtained in this range, since the type of crack growth changed from stable to unstable, as discussed in the text.)

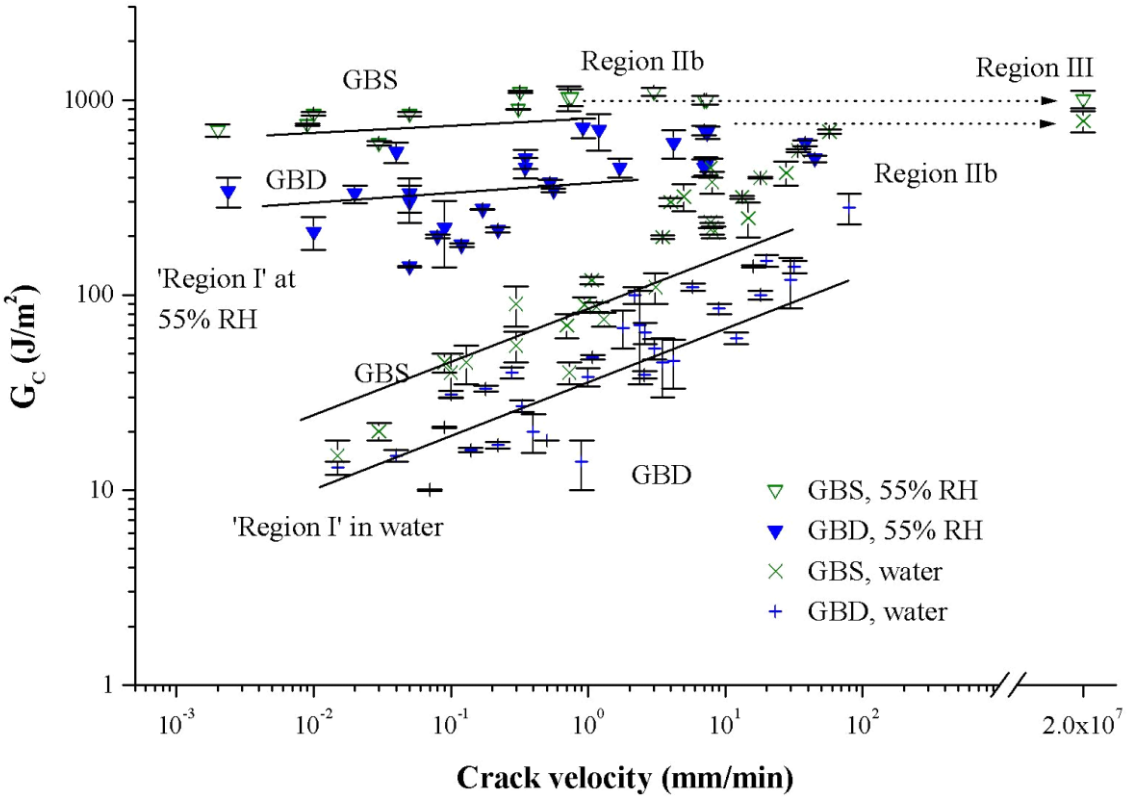

FIGURE 3 Relationship between the fracture energy, G_c, and the crack velocity, $\dot{a}$, for the 'GBD'- and 'GBS'-pretreated aluminium-alloy/steel dissimilar joints. Results are shown for tests conducted both at 21±1°C at 55% RH and in water. (In these figures the solid or dashed lines ending with an arrowhead indicate that no results could be obtained in this range, since the type of crack growth changed from stable to unstable, as discussed in the text.)

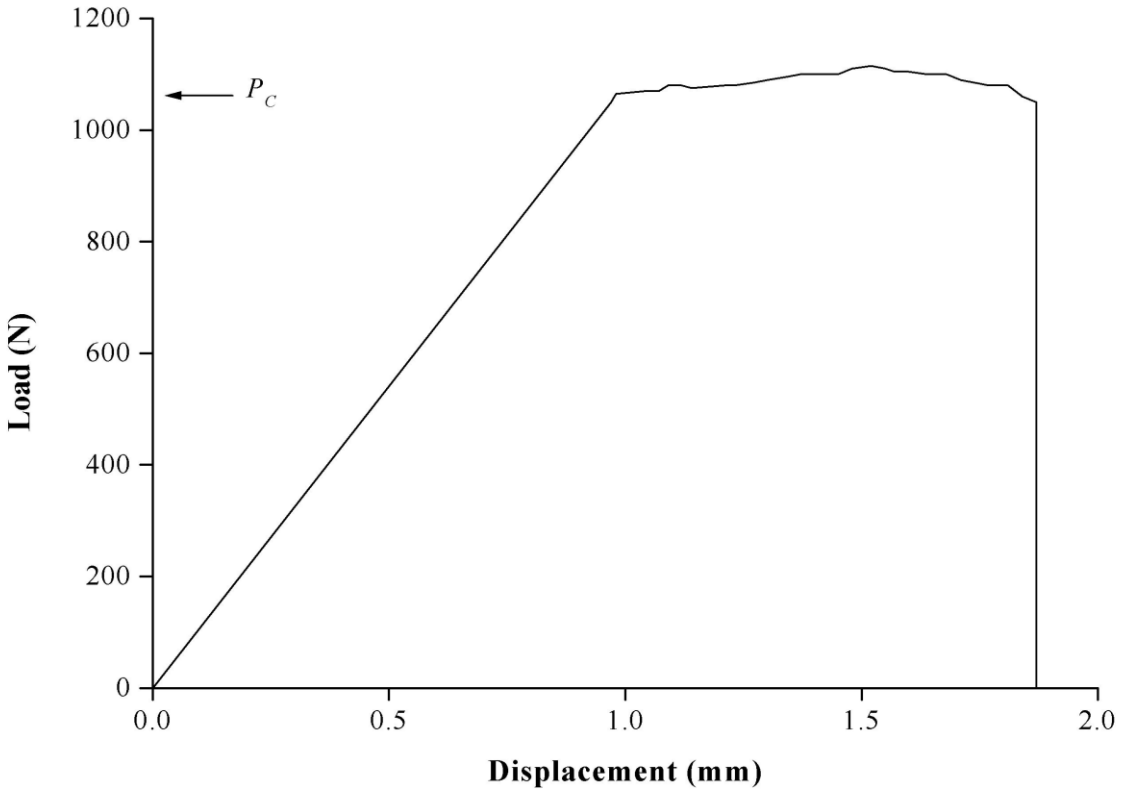

FIGURE 4 Typical load, *P*, versus displacement, *y*, curve associated with stable crack growth, as seen in 'Region I' (and 'Region II'). The specimen was a 'GBD'-pretreated steel joint tested at 0.1 mm/minute at 55%RH.

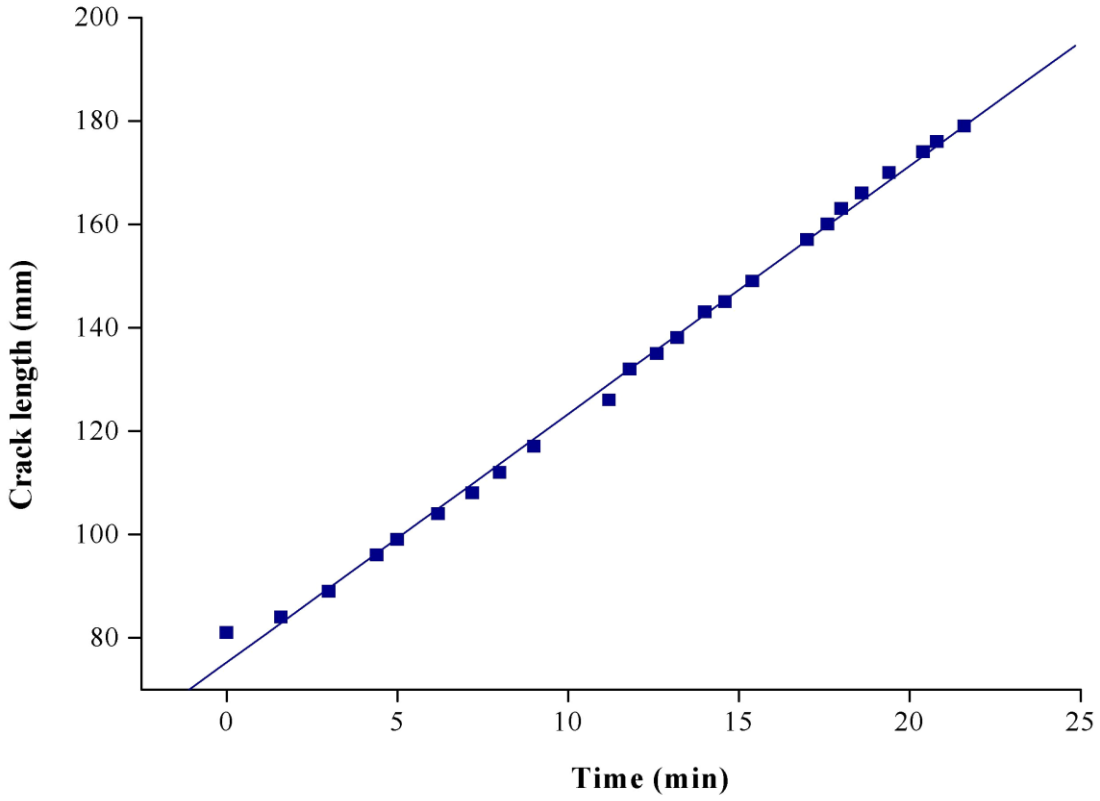

FIGURE 5 Relationship between crack length, *a*, and time, *t*, as seen in 'Region I'. The specimen was a 'GBD'-pretreated steel joint tested at 0.05 mm/minute at 55%RH.

6 (a)

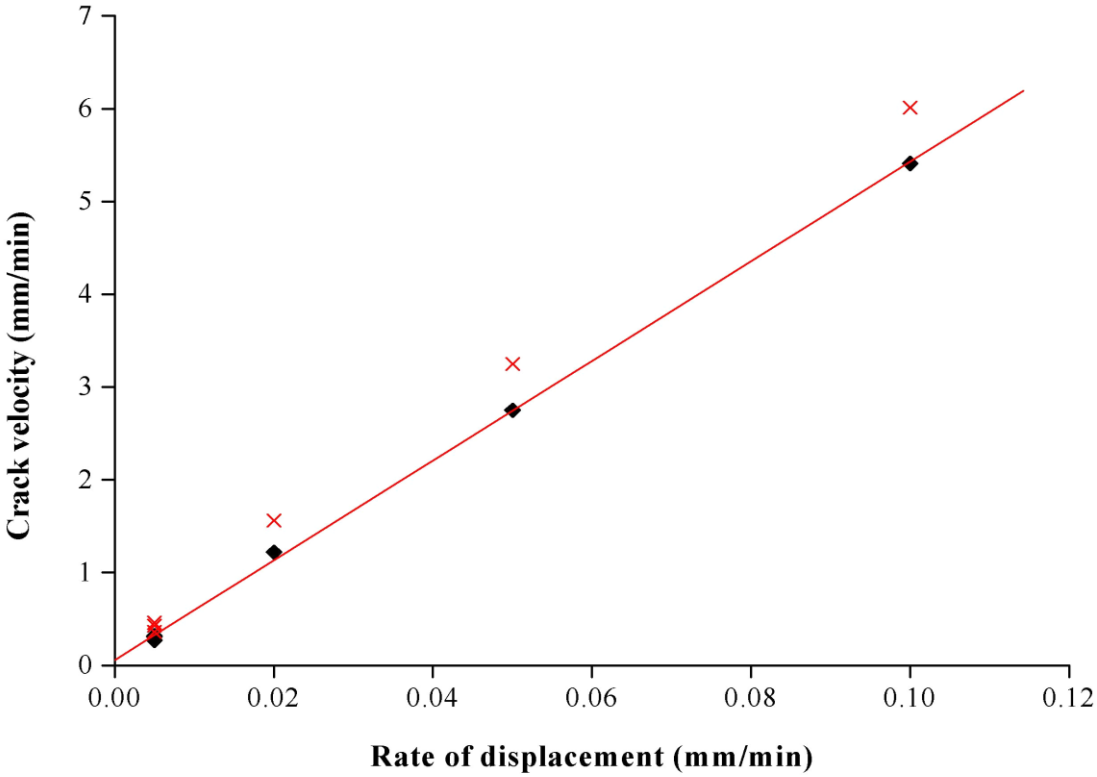
Crack velocity (mm/min)
Rate of displacement (mm/min)
0
1
2
3
4
5
6
7
0.00
0.02
0.04
0.06
0.08
0.10
0.12

6 (b)

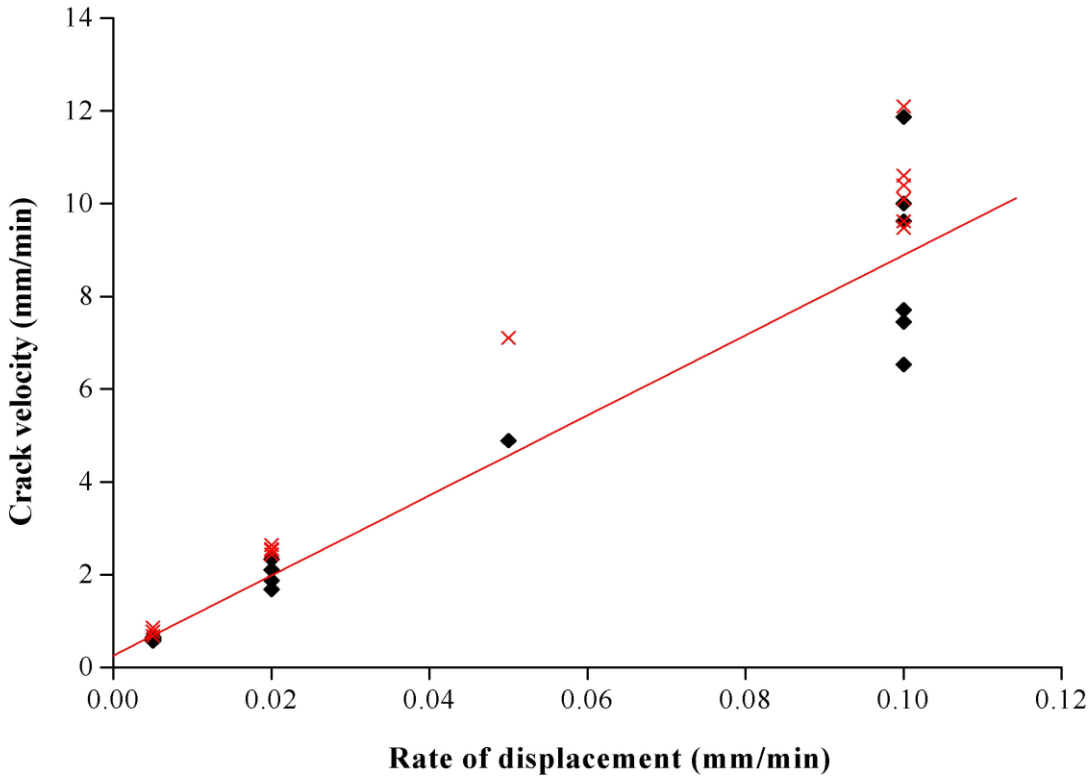

FIGUR E 6 Relationship between crack velocity, $\dot{a}$, and rate of displacement, $\dot{y}$, as seen in 'Region I' for the 'GBD'-pretreated (a) aluminium-alloy joints, and (b) steel joints. (For each type of substrate: ♦: experimental points; and x: points given by Equation (3). The straight line plotted represents the best statistical fit for the experimental data, as obtained via a linear regression analysis.)

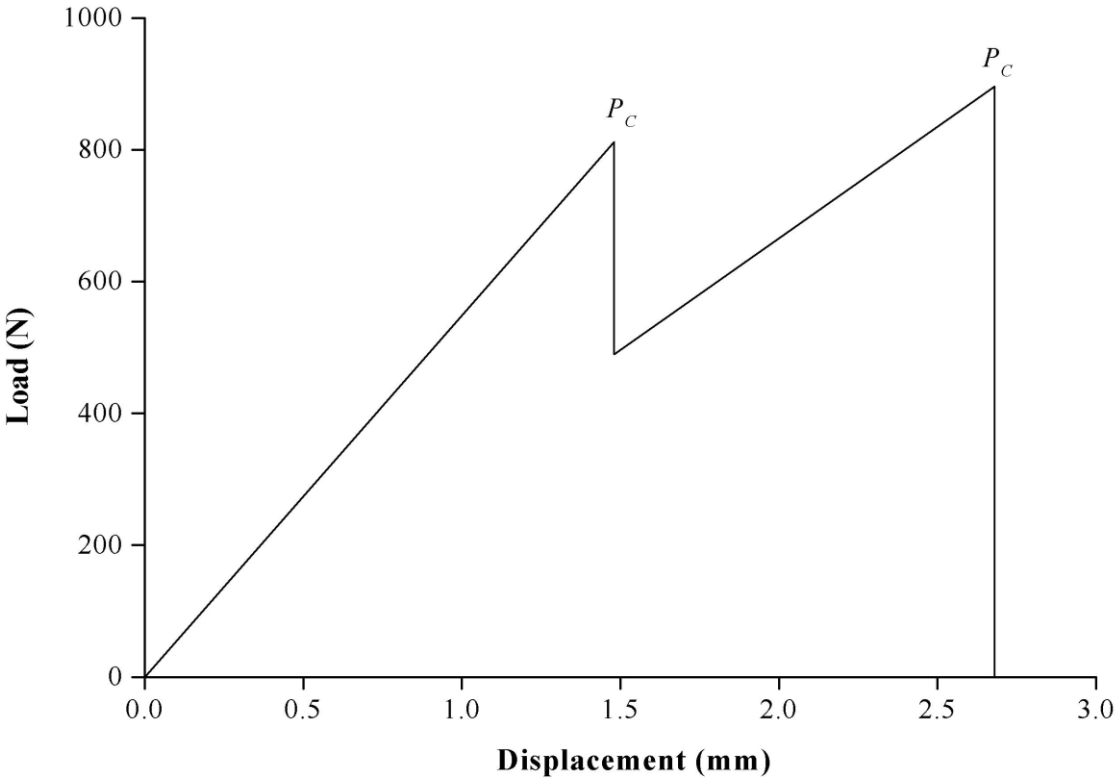

FIGURE 7 Typical load, *P*, versus displacement, *y*, curve associated with stick-slip crack growth, as seen in 'Region III'. The peaks correspond to crack initiation and the valleys to crack arrest. The specimen was a 'GBS'-pretreated aluminium-alloy joint tested at 0.1 mm/minute at 55%RH.

8 (a)

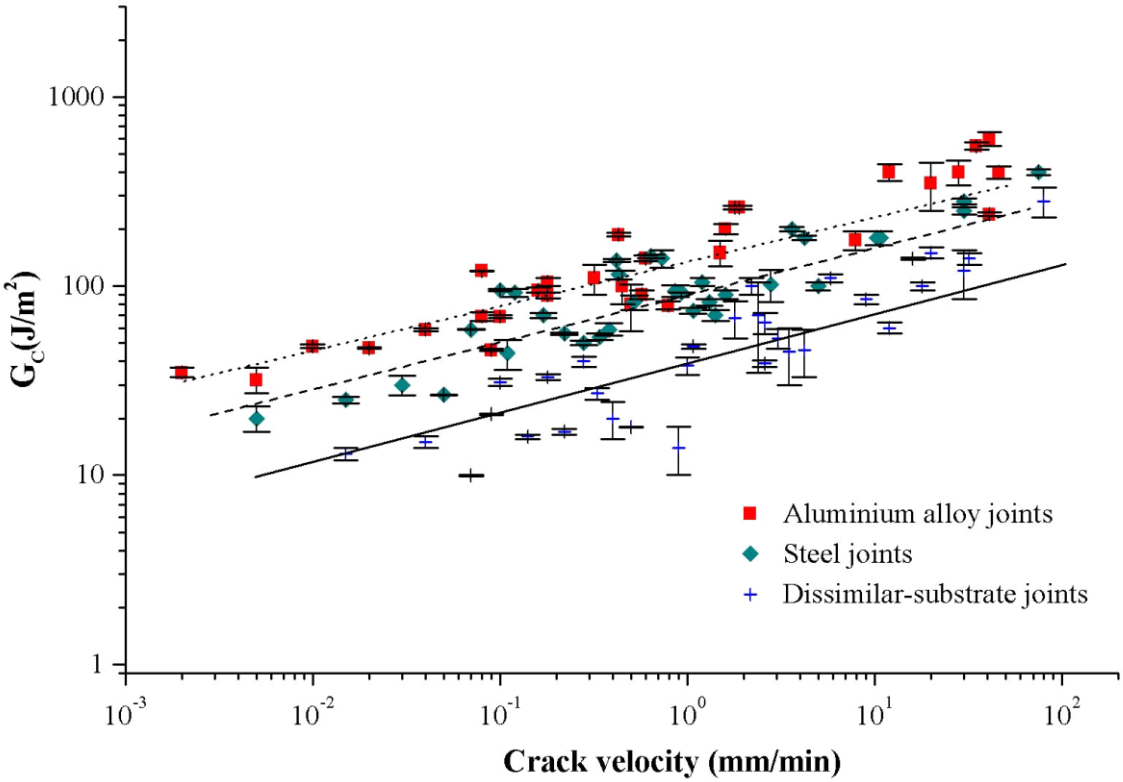
1000
100
10
1
G_C(J/m^2)
10^{-3}
10^{-2}
10^{-1}
10^{0}
10^{1}
10^{2}
Crack velocity (mm/min)
Aluminium alloy joints
Steel joints
Dissimilar-substrate joints

8 (b)

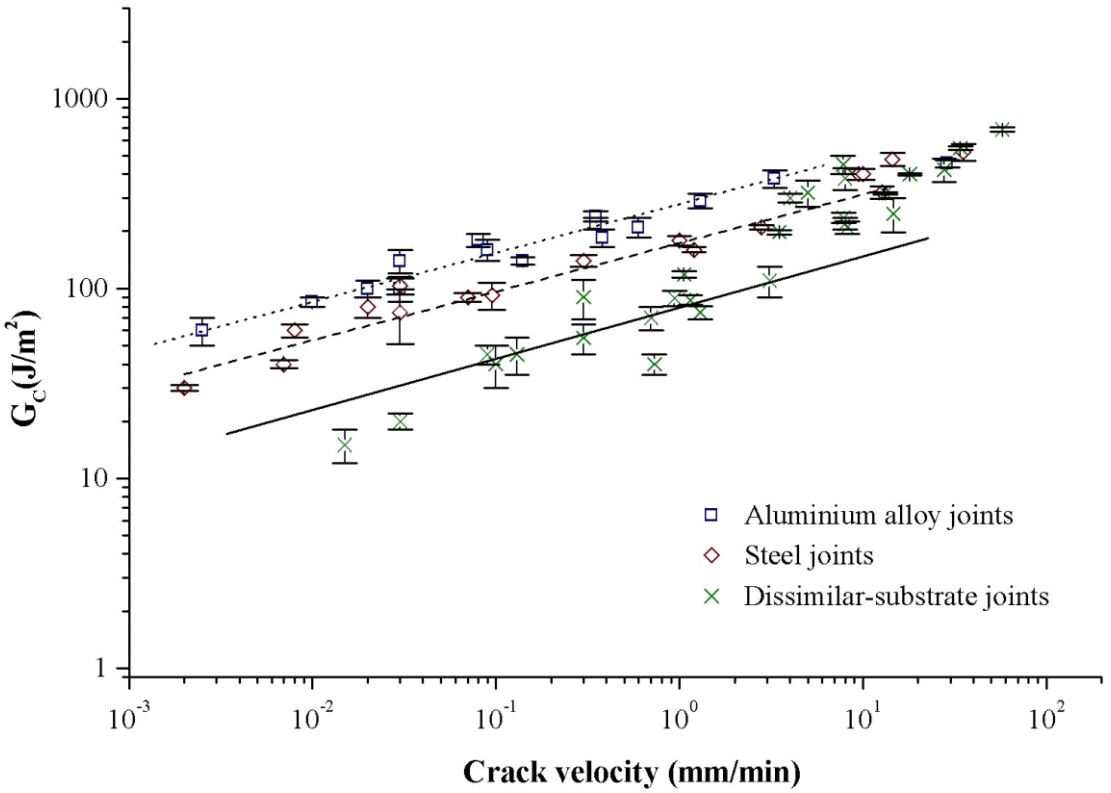

FIGURE 8 Relationship between the fracture energy, G_c, and the crack velocity, $\dot{a}$, for the (a) 'GBD'- and the (b) 'GBS'-pretreated joints in 'Region I' for the tests conducted in water.

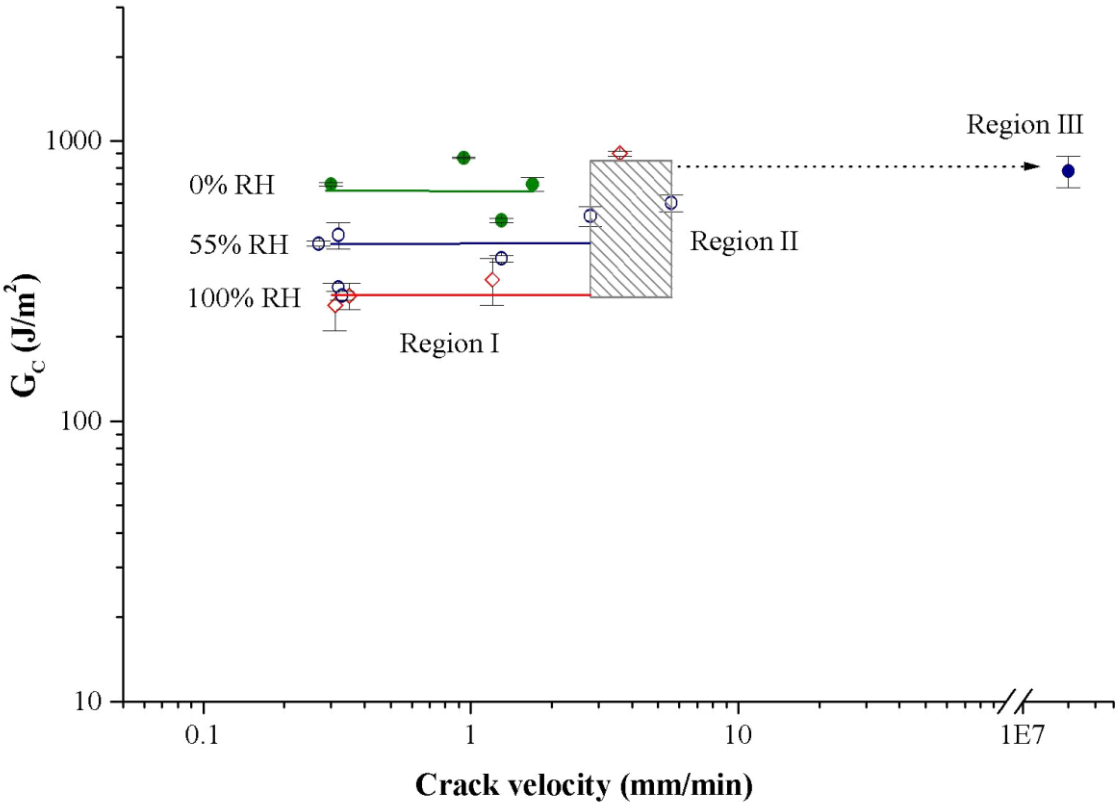

FIGURE 9 Relationship between the fracture energy, G_c, and the crack velocity, $\dot{a}$, for the 'GBD'-pretreated aluminium-alloy joints obtained at 0%, 55% and 100%RH. (Filled circles: 0%RH; open circles: 55%RH and open diamonds: 100%RH.)

10 (a)

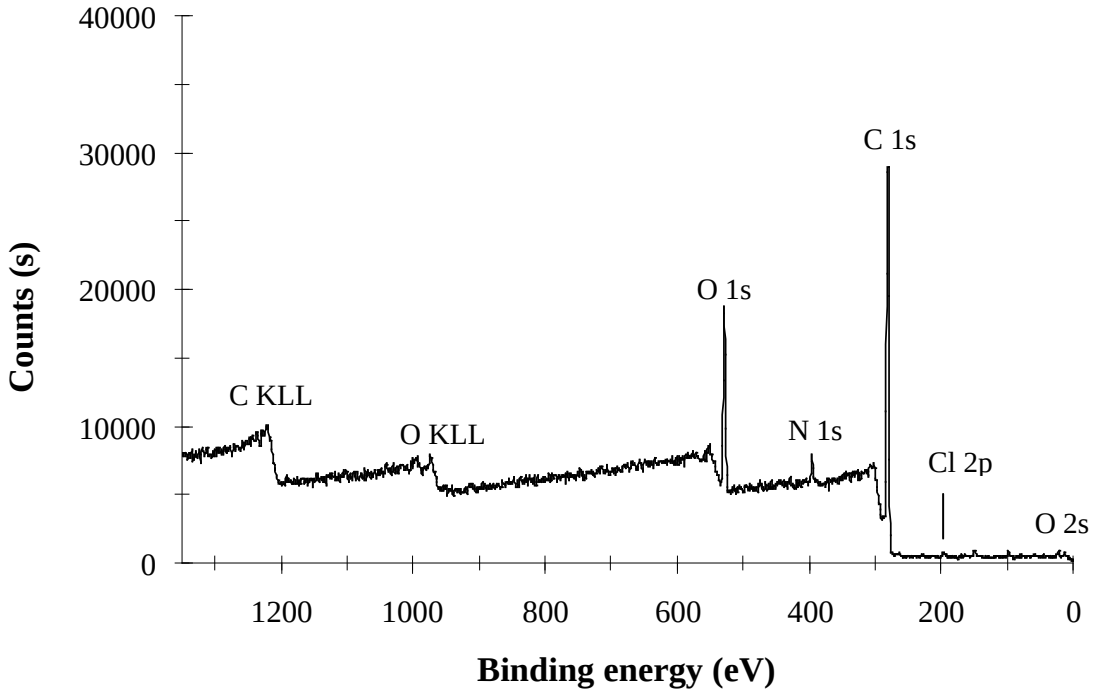
40000
30000
20000
10000
0
Counts (s)
C 1s
O 1s
C KLL
O KLL
N 1s
Cl 2p
O 2s
1200
1000
800
600
400
200
0
Binding energy (eV)

10 (b)

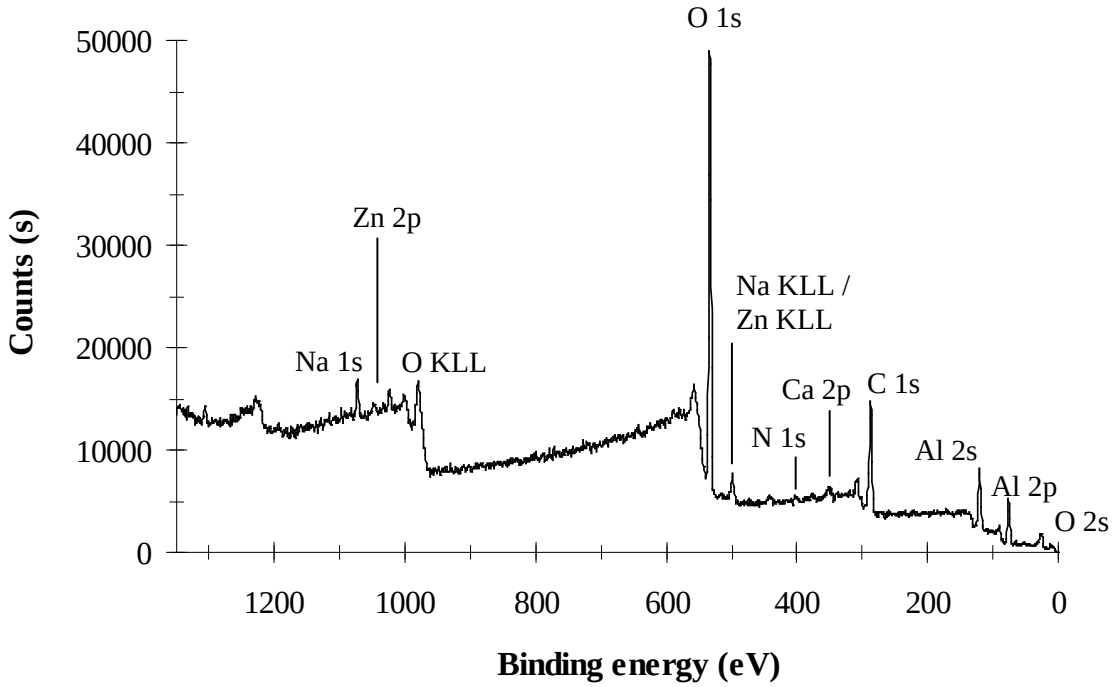
O 1s
50000
40000
30000
20000
10000
0
Counts (s)
Zn 2p
Na 1s
O KLL
Na KLL /
Zn KLL
Ca 2p
C 1s
N 1s
Al 2s
Al 2p
O 2s
1200
1000
800
600
400
200
0
Binding energy (eV)

10 (c)

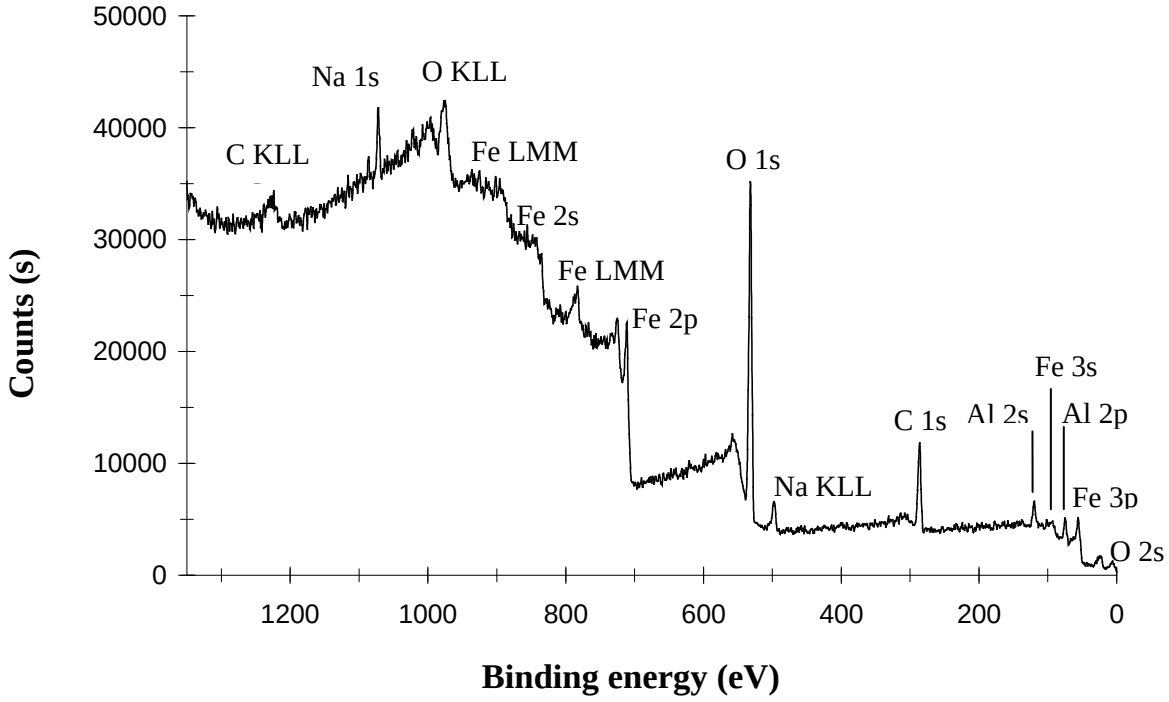

FIGURE 10 XPS survey spectra for "control" surfaces: (a) adhesive, (b) 'GBD'-pretreated aluminium-alloy, (c) 'GBD'-pretreated steel.

11 (a)

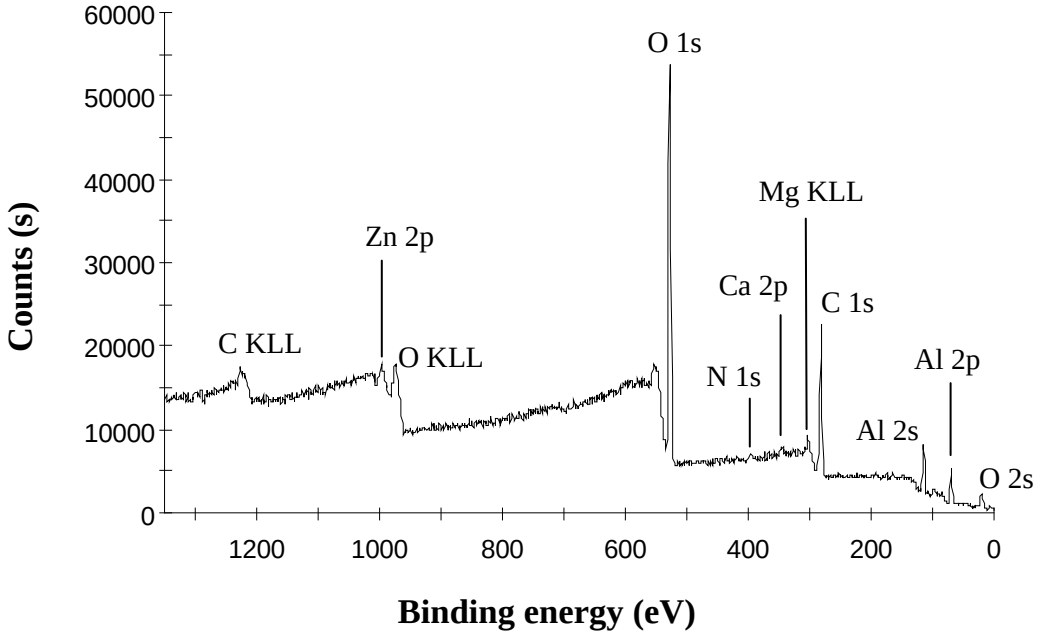
60000
50000
40000
30000
20000
10000
0
Counts (s)
O 1s
Mg KLL
Zn 2p
Ca 2p
C 1s
C KLL
O KLL
N 1s
Al 2p
Al 2s
O 2s
1200
1000
800
600
400
200
0
Binding energy (eV)

11 (b)

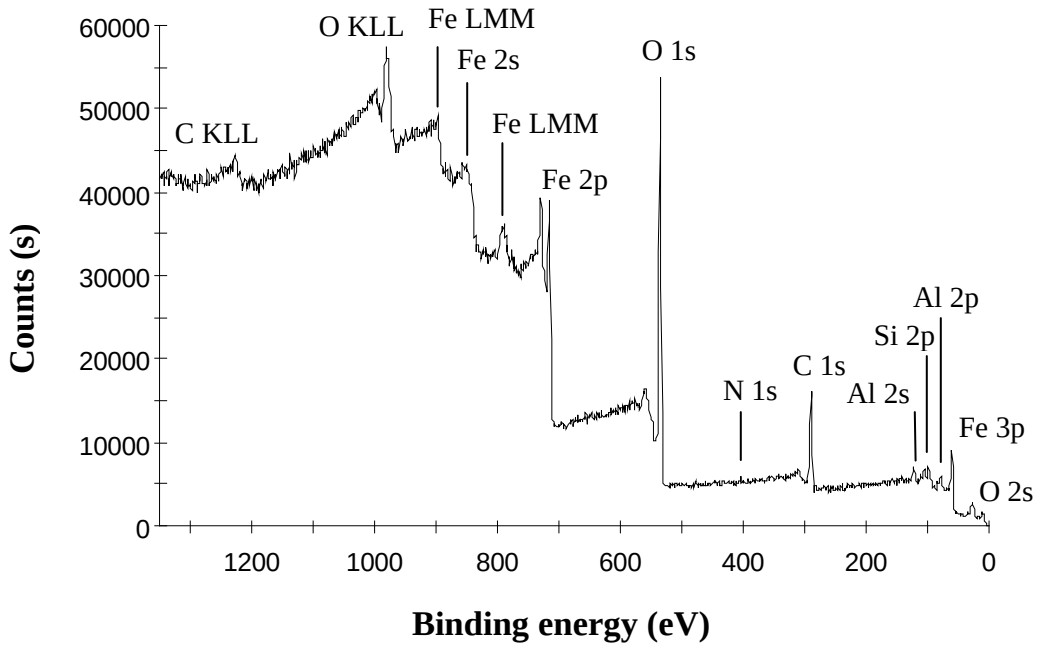

FIGURE 11 XPS survey spectra of the interfacial metal failure surfaces for similar substrate joints tested in water: (a) 'GBD'-pretreated aluminium-alloy, (b) 'GBD'-pretreated steel.

12 (a)

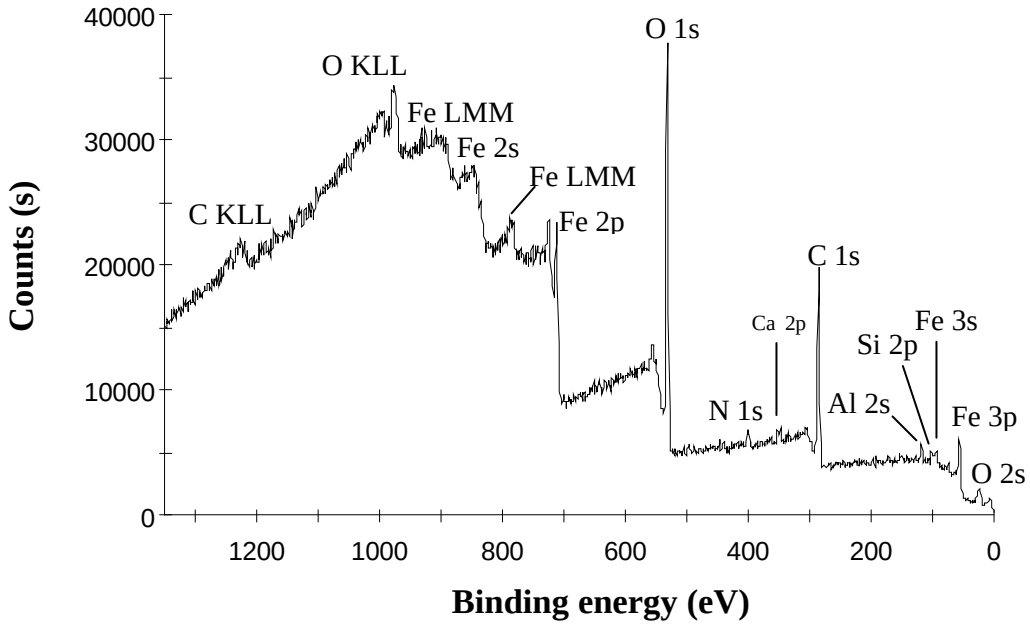
40000
30000
20000
10000
0
Counts (s)
1200
1000
800
600
400
200
0
Binding energy (eV)
O 1s
O KLL
Fe LMM
Fe 2s
Fe LMM
Fe 2p
C KLL
C 1s
Ca 2p
Fe 3s
Si 2p
N 1s
Al 2s
Fe 3p
O 2s

12 (b)

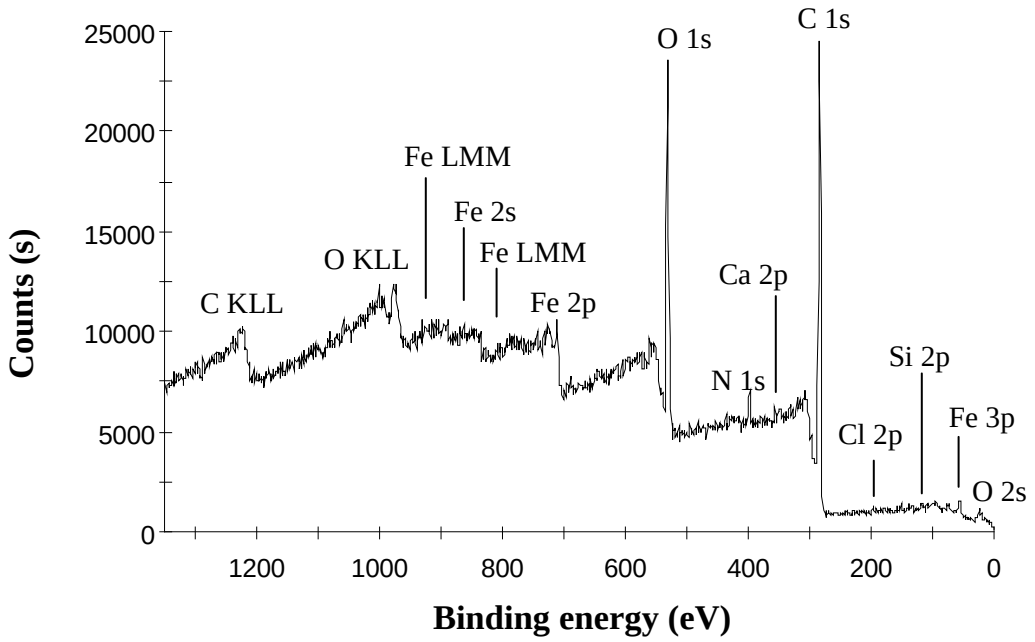

FIGURE 12 XPS survey spectra of the failure surfaces from the 'GBD'-pretreated dissimilar substrate joint tested in water: (a) the steel failure surface, (b) the adhesive failure surface.

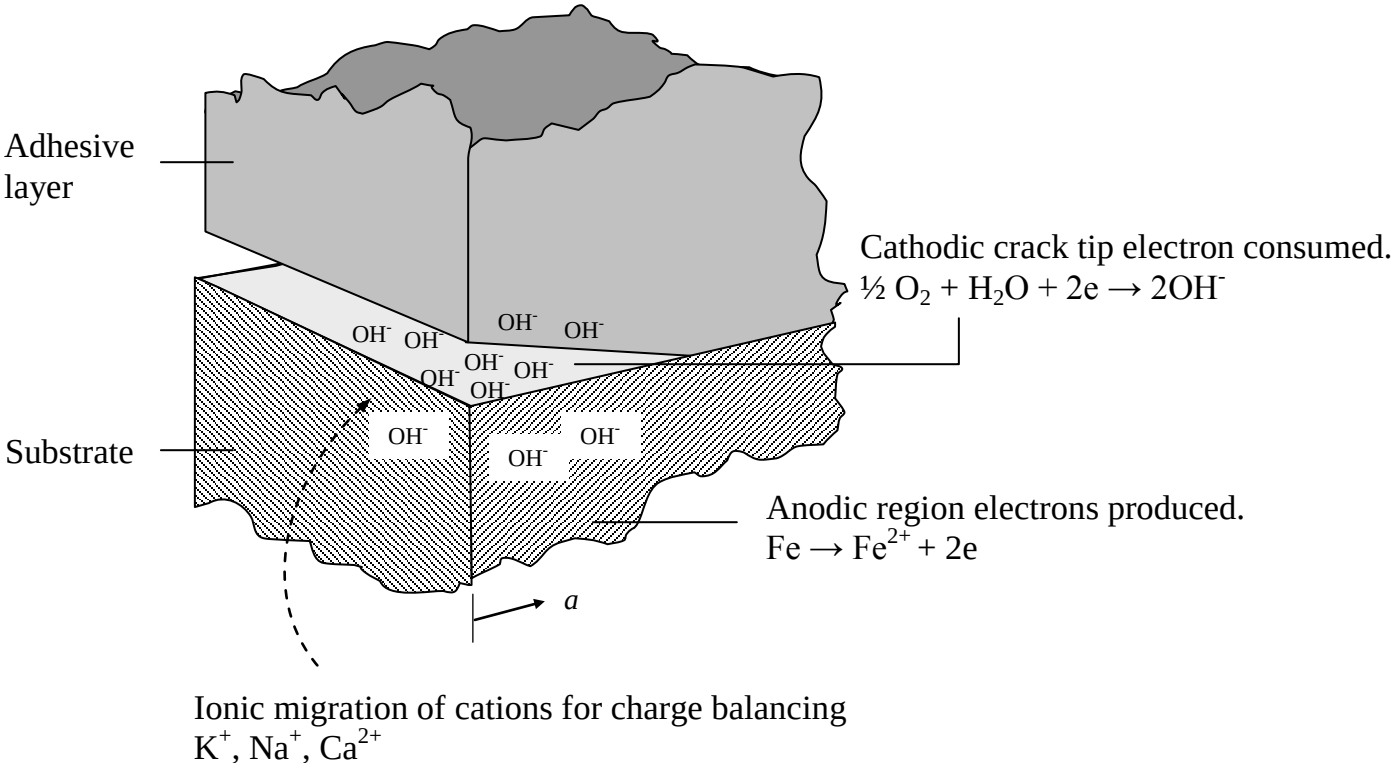

FIGURE 13 Schematic representation of the cathodic disbondment mechanism that is responsible for failure when joints are exposed to liquid water. The cathodic reduction of water at the crack tip produces hydroxide ions which lead to adhesion loss at the interface. Electrons required for this reaction must first be produced at the adjacent anodic site where metal dissolution occurs.

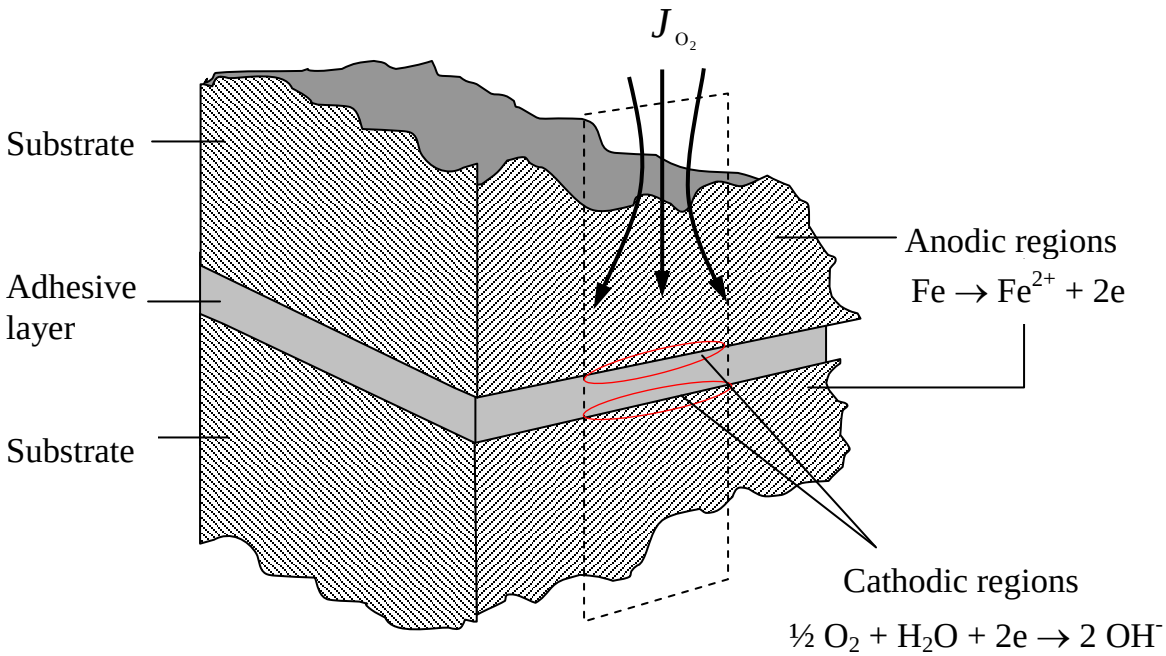

FIGURE 14 Schematic illustration of the supply of oxygen ($\boldsymbol{J_{O2}}$) to the crevice(s) developing at the adhesive-layer/substrate interface(s). As freshly aerated water arrives so it must supply oxygen to both crevices in the case of the steel/steel joint but only the steel/adhesive interface in the case of the dissimilar substrate joint.

15 (a)

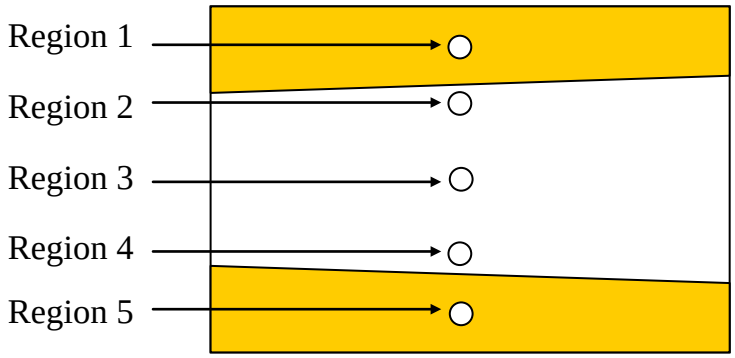
Region 1
Region 2
Region 3
Region 4
Region 5

15 (b)

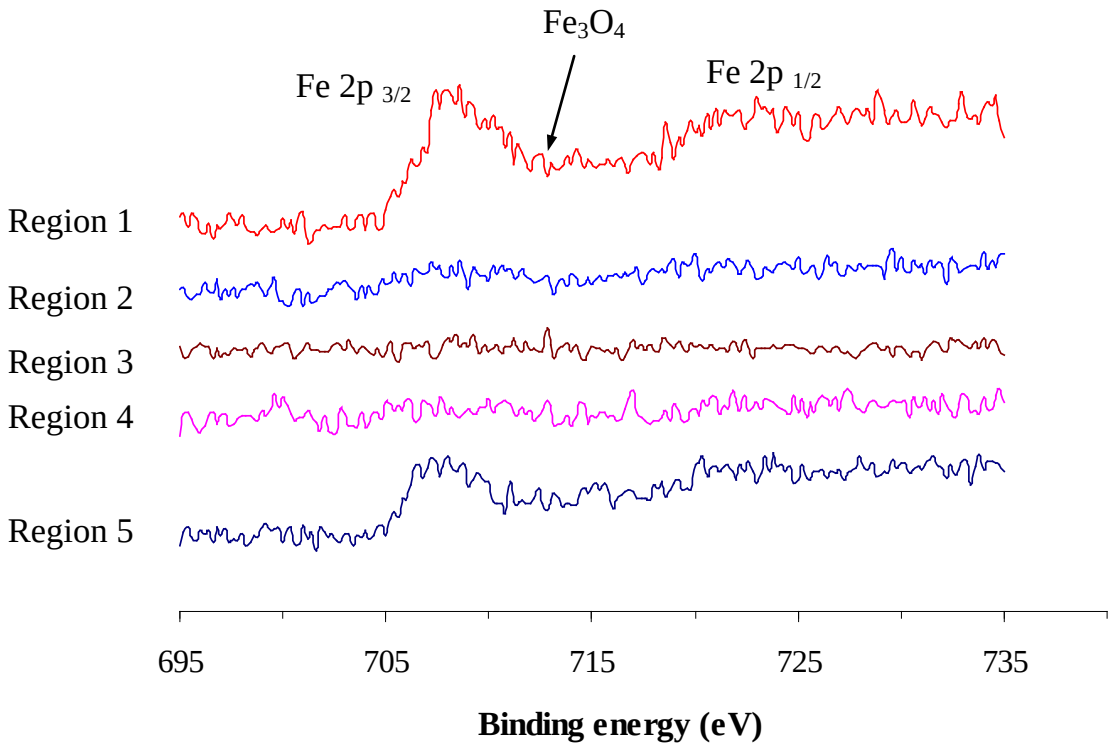
Fe3O4
Fe 2p 3/2
Fe 2p 1/2
Region 1
Region 2
Region 3
Region 4
Region 5
695
705
715
725
735
Binding energy (eV)

15 (c)

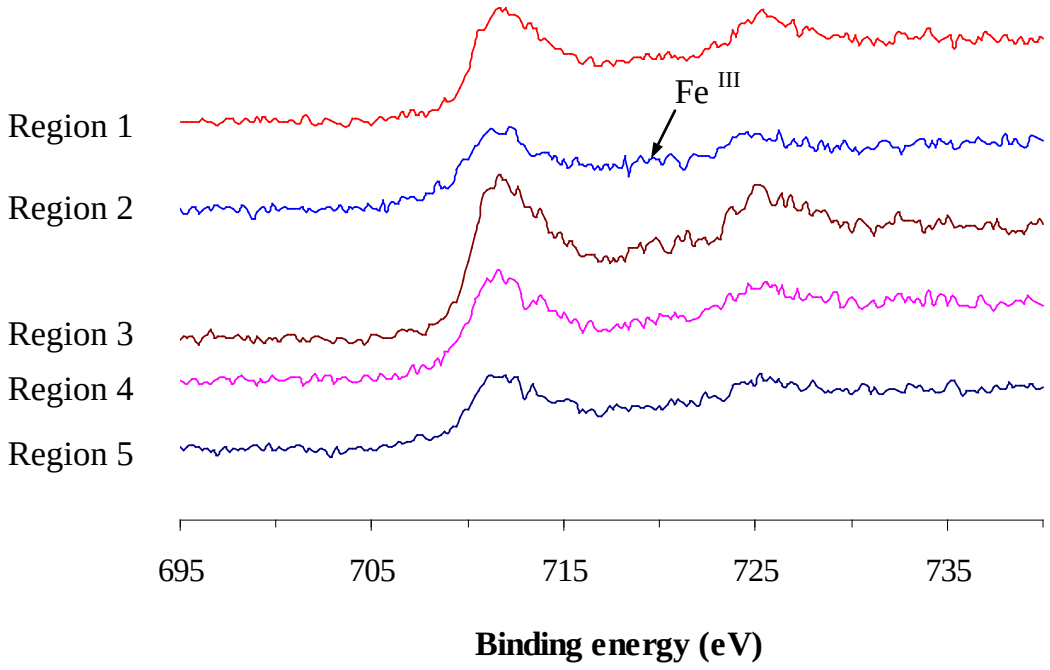

FIGURE 15 Evidence for iron residues on the adhesive side of the failed 'GBD'-pretreated steel joint. (a) Schematic appearance of adhesive failure surface at midpoint along the length of the TDCB specimen, showing positions for XPS analysis. (b) Fe2p XPS spectra from the regions of (a) showing the presence of iron near the edge of the specimen. (c) Complementary Fe2p spectra from equivalent positions on the steel side of the joint.

16 (a)

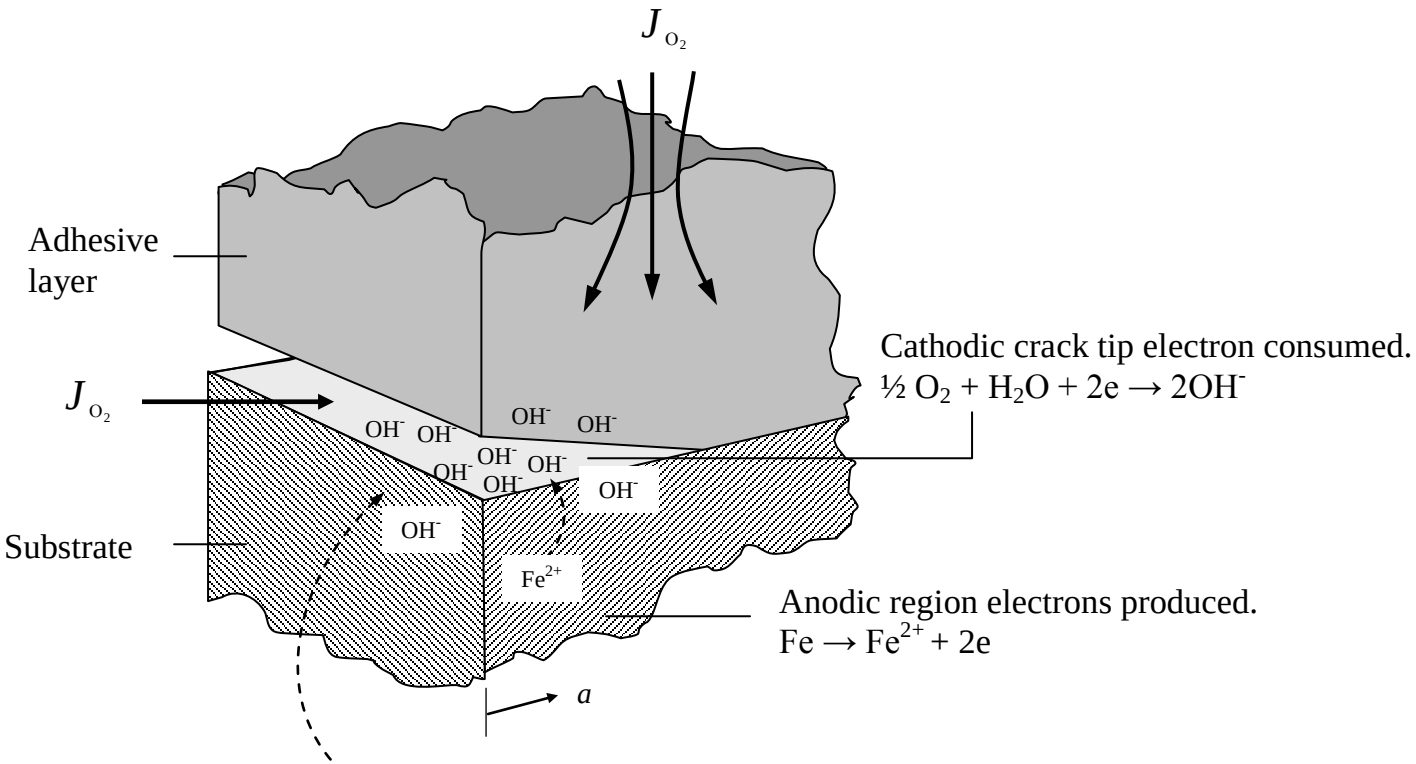
J_{O_2}
Adhesive layer
J_{O_2}
OH⁻ OH⁻ OH⁻ OH⁻
OH⁻ OH⁻ OH⁻ OH⁻
OH⁻
OH⁻
Substrate
Fe²⁺
a
Cathodic crack tip electron consumed.
½ O₂ + H₂O + 2e → 2OH⁻
Anodic region electrons produced.
Fe → Fe²⁺ + 2e
Ionic migration of cations for charge balancing
K⁺, Na⁺, Ca²⁺

16 (b)

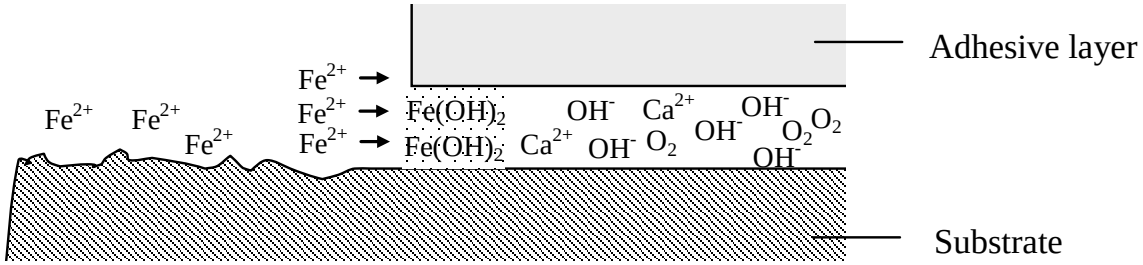

FIGURE 16 Schematic representation of the factors influencing supply of oxygen in the developing crevices. (a) In the early stages of failure oxygen is supplied at the advancing crevice tip as the crack proceeds along the length of the beam and also normal to the direction of crack growth to establish a small but significant developing crevice at the edge of the specimen. (b) The edge crevice may become blocked with corrosion products in this manner in the later stages of joint failure and thus have a disproportionate effect on the failure kinetics.

17 (a)

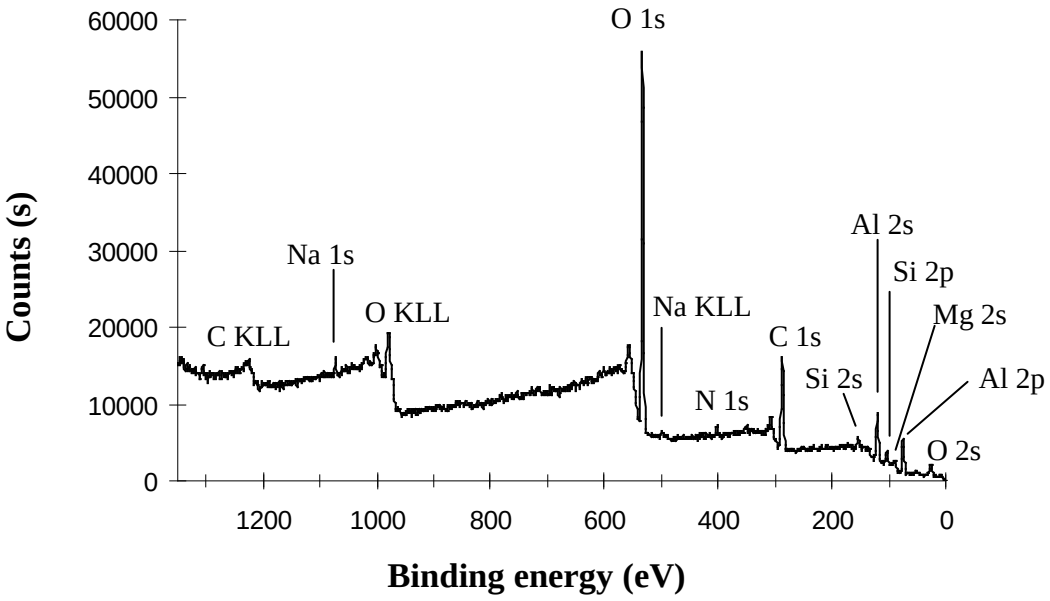
60000
50000
40000
30000
20000
10000
0
Counts (s)
1200
1000
800
600
400
200
0
Binding energy (eV)
O 1s
Na 1s
O KLL
C KLL
Na KLL
C 1s
N 1s
Si 2s
Al 2s
Si 2p
Mg 2s
Al 2p
O 2s

17 (b)

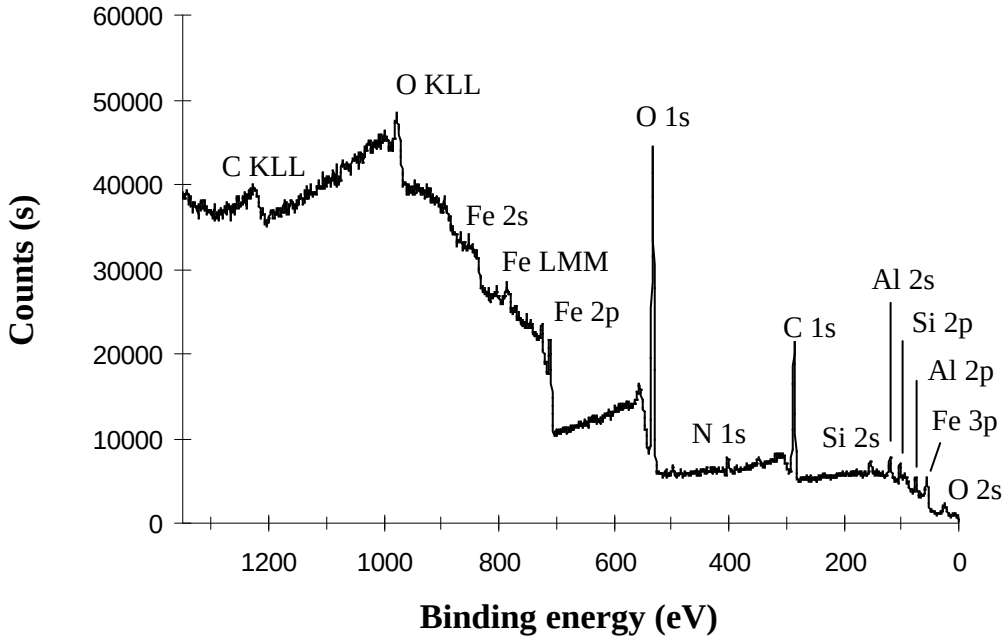

FIGURE 17 XPS survey spectra for the silane pretreated substrates: (a) 'GBS'-pretreated aluminium-alloy, (b) 'GBS'-pretreated steel.

18 (a)

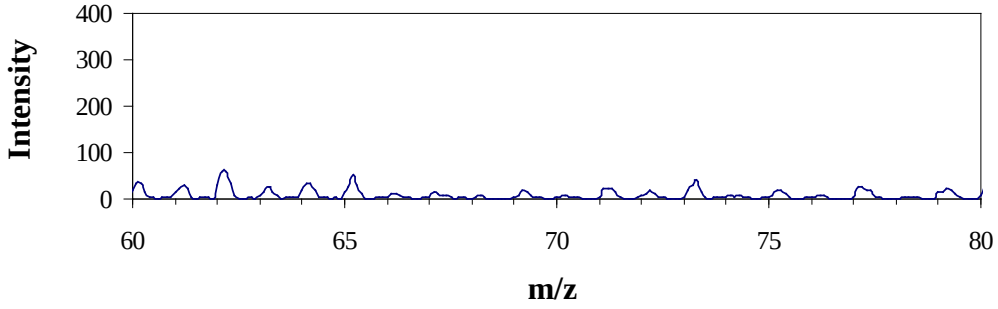

18 (b)

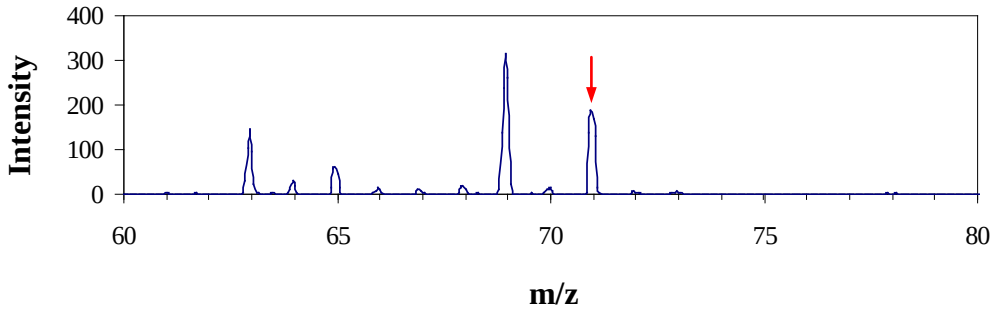

18 (c)

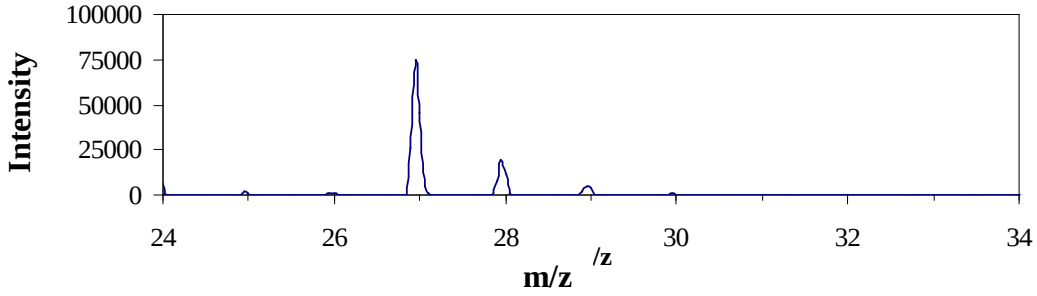

FIGURE 18 Positive ToF-SIMS spectra for aluminium-alloy substrate. (a) m/z = 60 – 80 for 'GBD' pretreatment, (b) m/z = 60 – 80 for 'GBS' pretreatment, the arrowed peak at m/z = 71 is assigned to $SiOAl^+$, (c) m/z = 24 -34 for 'GBS' pretreatment, the peak at m/z = 27 is Al^+.

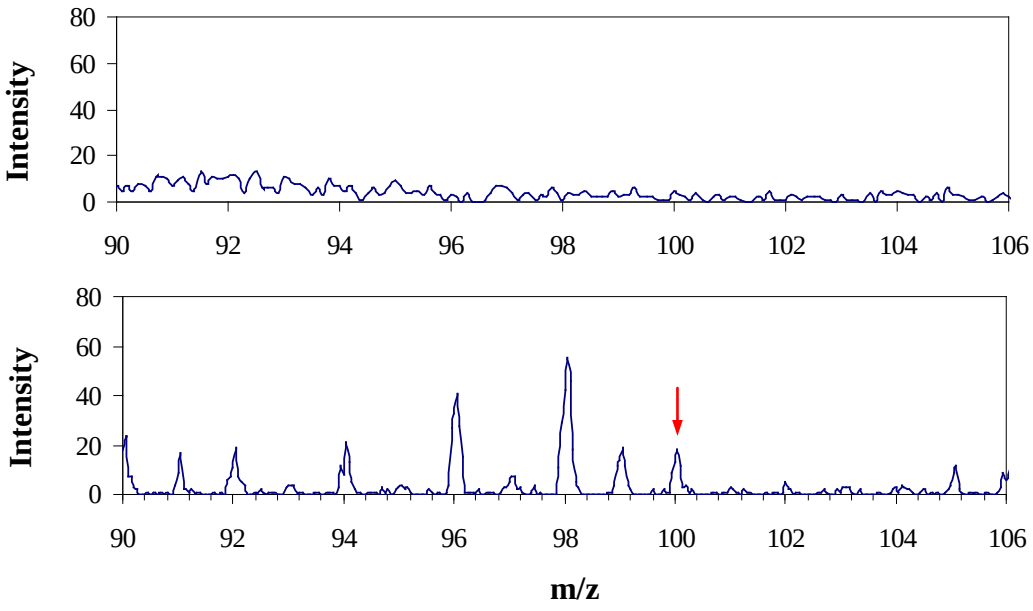

FIGURE 19 Positive ToF-SIMS spectra in the mass range m/z = 90 – 106 for the 'control' steel substrates: (a) a 'GBD' pre-treatment, (b) a 'GBS' pretreatment, the arrowed peak at m/z = 100 is assigned to $FeOSi^+$.

20 (a)

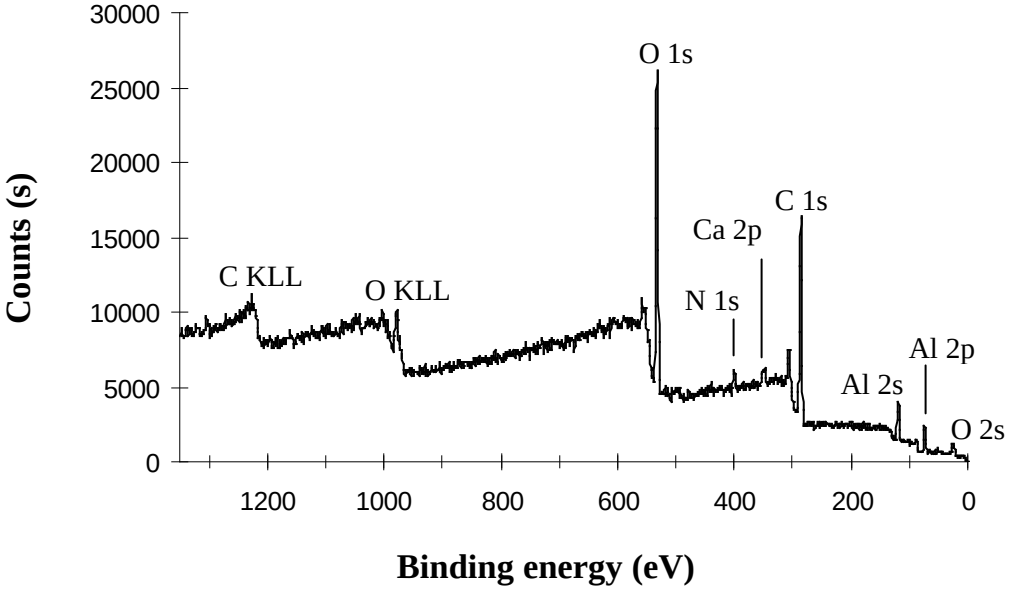

20 (b)

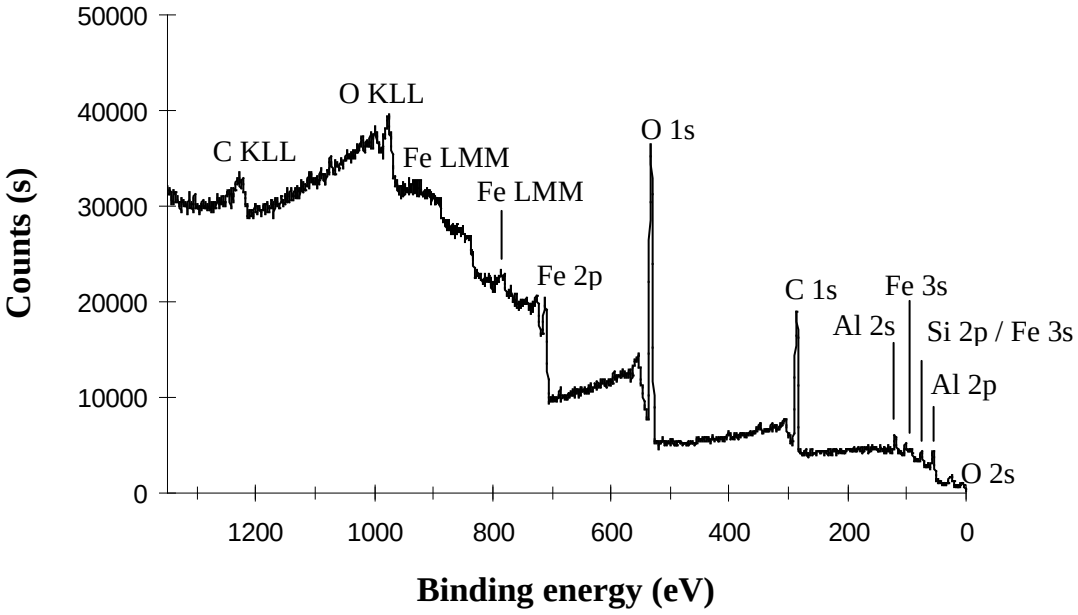

FIGURE 20 XPS survey spectra of the interfacial metal failure surfaces for the silane treated similar substrate joints tested in water: (a) 'GBS'-pretreated aluminium-alloy, (b) 'GBS'-pretreated steel.